

1 **Insights into characteristics, sources and evolution of submicron aerosols**
2 **during harvest seasons in Yangtze River Delta (YRD) region, China**

3

4 **Y. J. Zhang^{1,2}, L. L. Tang^{2,1}, Z. Wang¹, H. X. Yu³, Y. L. Sun⁴, D. Liu⁵, W. Qin²,**
5 **F. Canonaco⁶, A. S. H. Prévôt⁶, H. L. Zhang⁷, and H.-C. Zhou¹**

6

7 ¹Jiangsu Key Laboratory of Atmospheric Environment Monitoring and Pollution Control,
8 School of Environmental Science and Engineering, Nanjing University of Information
9 Science and Technology, Nanjing 210044, China

10 ²Jiangsu Environmental Monitoring Center, Nanjing 210036, China

11 ³State Key Laboratory of Pollution Control and Resource Reuse, School of the Environment,
12 Nanjing University, Nanjing 210093, China

13 ⁴State Key Laboratory of Atmospheric Boundary Layer Physics and Atmospheric Chemistry,
14 Institute of Atmospheric Physics, Chinese Academy of Sciences, Beijing 100029, China

15 ⁵Centre for Atmospheric Science, School of Earth, Atmospheric and Environmental Sciences,
16 University of Manchester, Manchester M13 9PL, UK

17 ⁶Laboratory of Atmospheric Chemistry, Paul Scherrer Institute, Villigen PSI 5232,
18 Switzerland

19 ⁷Handix LLC, Boulder, CO 8031, USA

20 *Correspondence to:* L. L. Tang (lily3258@163.com)

21

22 **Abstract**

23 Atmospheric submicron particulate matter (PM₁) is one of the most significant pollution
24 components in China. Despite its current popularity in the studies of aerosol chemistry, the
25 characteristics, sources and evolution of atmospheric PM₁ species are still poorly understood
26 in China, particularly for the two harvest seasons, namely the summer wheat harvest and
27 autumn rice harvest. An Aerodyne Aerosol Chemical Speciation Monitor (ACSM) was
28 deployed for online monitoring of PM₁ components during summer and autumn harvest
29 seasons in urban Nanjing, in the Yangtze River Delta (YRD) region of China. PM₁
30 components were shown to be dominated by organic fraction (OA, 39% and 41%) and nitrate
31 (23% and 20%) during the harvest seasons (the summer and autumn harvest). Positive matrix
32 factorization (PMF) analysis of the ACSM OA mass spectra resolved four OA factors:
33 hydrocarbon-like mixed with cooking related OA (HOA + COA), fresh biomass burning OA
34 (BBOA), oxidized biomass burning-influenced OA (OOA-BB), and highly oxidized OA
35 (OOA); in particular the oxidized BBOA contributes ~80% of the total BBOA loadings. Both
36 fresh and oxidized BBOA exhibited apparent diurnal cycles with peak concentration at night,
37 when the high ambient relative humidity and low temperature facilitated the partitioning of
38 semi-volatile organic species [into the particle phase](#). The fresh BBOA concentrations for the
39 harvests are estimated as $BBOA = 15.1 \times (m/z\ 60 - 0.26\% \times OA)$, $m/z\ 60$ as a marker for
40 levoglucosan-like species. The $(BBOA + OOA-BB)/\Delta CO$, (ΔCO is the CO minus
41 background CO), decreases as a function of f_{44} (fraction of $m/z\ 44$ in OA signal), which might
42 indicate that BBOA was oxidized to less volatile OOA, e.g., more aged and less volatile OOA
43 (LV-OOA) during the aging process. Analysis of air [mass back-trajectories](#) indicates that the
44 high BB pollutant concentrations are linked to the air masses from the western (summer
45 harvest) and southern (autumn harvest) areas.

46

47 **1 Introduction**

48 Particulate matter (PM) that is suspended in the atmosphere as atmospheric aerosol plays a
49 crucial role in regional and global climate system (Ramanathan et al., 2001; Kaufman et al.,
50 2002), air pollution (Sun et al., 2013), ambient visibility reduction (Watson, 2002) and human
51 health (Ge et al., 2011). Significant amounts of PM can be generated from human activities.
52 In particular, biomass burning (BB) activities, e.g., forest fires, wildfire, and agricultural fires,
53 can become the main sources of fine particulate matter (PM_{2.5}, particulates $\leq 2.5 \mu\text{m}$ in
54 aerodynamic diameter) and/or submicron particulate matter (PM₁, particulates $\leq 1 \mu\text{m}$ in
55 aerodynamic diameter) (Andreae and Merlet, 2001, Aiken et al., 2010; DeCarlo et al., 2010;
56 Lee et al., 2010; Cubison et al., 2011; Reche et al., 2012; Bougiatioti et al., 2014).
57 Agricultural residues burning is one of the most serious sources leading to severe air quality
58 problems during harvest seasons in China (Li et al., 2007; Wang et al., 2009a; Du et al., 2011;
59 Cheng et al., 2013; Ding et al., 2013). Moreover, China is an agricultural country which has
60 1.8 billion cultivated fields with a large amount of agricultural crop residue (Zhang et al.,
61 2008). Recently, the use of agricultural residues as fuel in China declined. During harvest
62 seasons, farmers usually harvest the crop in the daytime and burn agricultural residues in
63 their fields directly, which results in BB emissions. The investigation of the compositions,
64 sources and processes of atmospheric aerosol particles during harvest seasons is urgently
65 needed to better understand the impact of aerosol particles from BB sources on air quality.

66 Organic aerosol (OA) composes a large fraction of atmospheric aerosol particles (Zhang
67 et al., 2007). Combination of positive matrix factorization (PMF, Paatero, 1997) and a PMF
68 Evaluation Toolkit (PET, Ulbrich et al., 2009) has been well used to identify and apportion
69 the sources of OA in recent studies (e.g. Lanz et al., 2007; Ulbrich et al., 2009; Allan et al.,
70 2010; Zhang et al., 2005a, 2011; Crippa et al., 2013, 2014; Sun et al., 2013). In addition, an
71 IGOR-based Source Finder (SoFi, Canonaco et al., 2013) with a multilinear engine algorithm

72 (ME-2, Paatero, 1999) can also resolve the emission sources of OA. The current PMF and
73 ME-2 method can only be employed to analyze OA datasets a posteriori (Sun et al., 2012;
74 Zhang et al., 2011; Canonaco et al., 2013), but cannot be easily utilized in the real-time
75 online estimation of atmospheric OA sources. To identify the sources of atmospheric OA
76 online, an algorithm based solely on organic mass fragments, namely m/z 57 (mostly $C_4H_9^+$)
77 and m/z 44 (mostly CO_2^+), was developed to estimate hydrocarbon-like OA (HOA) and
78 oxygenated OA (OOA), respectively (Zhang et al., 2005a, 2005b; Ng et al., 2011c). Mohr et
79 al. (2012) also identified cooking OA (COA) in ambient datasets based on the fractions of
80 COA tracers at m/z 55 (mostly $C_4H_7^+$) and m/z 57 organic mass fragments. Biomass burning
81 organic aerosol (BBOA) is one of the major atmospheric OA species during BB periods
82 (Aiken et al., 2010; Allan et al., 2010). However, limited information on developing the
83 tracer-based method a posteriori is available for estimating the source apportionment of
84 BBOA.

85 The evolution processes of atmospheric OA, e.g., aging and/or [oxidation](#), can
86 significantly influence the physicochemical properties of OA (Aiken et al., 2008; Jimenez et
87 al., 2009; Sun et al., 2011b). In the presence of BB source, various volatile and semi-volatile
88 organic precursors can be emitted from the field burning of agricultural wastes, and SOA can
89 be formed from these precursors rapidly (Jimenez et al. 2009; Grieshop et al., 2009; Heringa
90 et al., 2011; Kawamura et al., 2013). What is more, BB plumes can be mixed with urban and
91 regional pollutants during aging processes (DeCarlo et al., 2010; Cubison et al., 2011). In
92 addition, the secondary formation, atmospheric transport and diffusion, as well as the mass
93 loadings and oxidation state of ambient OA can be also affected by the aging processes of
94 OA (Jimenez et al., 2009; Cubison et al., 2011; Sun et al., 2011b). Thus, it is important for
95 understanding the nature of atmospheric OA to investigate the evolution of OA and the
96 evolution process effects.

97 This study investigates the characteristics of PM₁ species using an Aerodyne Aerosol
98 Chemical Speciation Monitor (ACSM), and OA mass spectra are analyzed with PMF model
99 during summer and autumn harvests in the YRD region; the evolution of OA and the effects
100 of the evolution process on PM burden were also investigated. Combination of
101 back-trajectory analysis and local wind meteorology was used to investigate the origins.

102

103 **2 Experimental methods**

104 **2.1 Sampling site description**

105 With a population of more than 8 million and an area of ~ 6597 km², Nanjing, is a
106 representative Chinese city in terms of the pollution characteristics of the YRD region. Local
107 and regional air pollution events frequently occur in Nanjing, mainly caused by emissions of
108 mixed aerosols from fossil fuel burning, residential activities, and agricultural residues
109 burning (Wang et al., 2009a; Ding et al., 2013). In this study, all kinds of data was collected
110 in urban Nanjing (118°46'N, 32°05'E) from June 1 to 15, and October 15 to 30, 2013,
111 corresponding to two harvest seasons in a year, namely the summer wheat harvest and
112 autumn rice harvest. The sampling site was located on the roof of a six-story building
113 approximately 18 m above ground level, ~15 m from the nearest heavy-traffic road, and ~50
114 m from the nearest restaurants and residents. As a matter of fact, there is no agricultural field
115 in the urban Nanjing areas. However, there are some agricultural fields in the rural areas
116 around Nanjing (Figure S1). This means that the urban Nanjing site is significantly
117 influenced by the BB plumes originated from the rural areas. In addition, the local cooking
118 and traffic emissions can also significantly affect the PM pollution in this sampling site.
119 Therefore, in the presence of BB plumes, the mixed/complicated air pollution will occur in
120 urban Nanjing during the harvest seasons.

121

122 **2.2 Instrumentation and data analysis**

123 **2.2.1 Measurements**

124 The ambient non-refractory submicron aerosol (NR-PM₁) species, i.e., OA, nitrate, sulfate,
125 ammonium, chloride, were continuously measured using ACSM from June 1 to 15, and
126 October 15 to 30, 2013. In addition, the measurement without significant agricultural burning
127 impacts (little/negligible BB-influence) was also performed [at the same site](#) from July 1 to 8.
128 Detailed descriptions of ACSM can be found in previous studies (Ng et al., 2011a; Sun et al.,
129 2012). Briefly, the ambient aerosols were drawn into the room using a ½ inch (outer diameter)
130 stainless steel tube at a flow rate of ~3 l min⁻¹, of which ~84 cm³ min⁻¹ was sub-sampled into
131 the ACSM. Moreover, ACSM was operated at a time resolution of about 15 min with a scan
132 from *m/z* 10 to 150 amu at 500 ms amu⁻¹ rate, which corresponds to the settings of Sun et al.
133 (2012).

134 An online analyzer, Monitoring of Aerosols and Gases (MARGA, model ADI 2080
135 Applikon Analytical B. V. Corp., the Netherlands), was deployed to measure the mass
136 concentrations of a major water-soluble inorganic ion (potassium ion, K⁺) in the aerosols. A
137 PM_{2.5} cyclone inlet was used to remove coarse particles. Ambient air was sampled into a
138 liquid with a flow rate of 16.7 l min⁻¹. The detection limit of K⁺ is 0.09 µg m⁻³. The MET
139 ONE BAM-1020 and the 7-wavelength aethalometer (Magee AE31) were also employed to
140 measure PM₁ and ambient atmospheric BC in PM_{2.5}, respectively. CO was measured using a
141 gas analyzer (Thermo Scientific, Model 48i). Ambient meteorological parameters including
142 ambient temperature (*T*), relative humidity (RH), precipitation, wind speed (WS), and wind
143 direction (WD) were obtained from a ground level meteorology station located on the same
144 six-story building as the sampling site.

145 Daily fire locations used in this study were available from MODIS (Moderate-resolution
146 Imaging Spectroradiometer) mounted on NASA's Terra and Aqua satellites, NASA's Earth

147 Observing System (EOS) (<https://earthdata.nasa.gov/data/near-real-time-data/firms>). MODIS
148 can present fire distributions in details at 1 km resolution through Fire Information for
149 Resource Management System (FIRMS) on global scale (Justice et al., 2002; Kaufman et al.,
150 2003). As shown in Figure S1 – S2, all agricultural fire locations (red dots) in the YRD
151 region were detected by the remote sensing retrieval of MODIS from June 1 to 15, and
152 October 15 to 30, 2013 (<https://firms.modaps.eosdis.nasa.gov/firemap/>).

153

154 **2.2.2 ACSM data analysis**

155 An ACSM Data Analysis Software package, ACSM Local (Ver. 1.5.2.0.0, released April 25,
156 2012) written in Wavemetrics IgorTM, was used to analyze the ACSM dataset. More details of
157 procedures have been described in the studies of Ng et al. (2011a) and Sun et al. (2012). The
158 ACSM calibration is based on a combination of a Differential Mobility Analyzer (DMA, TSI
159 model 3080) and Condensation Particle Counter (CPC, TSI model 3775) for the ionization
160 efficiency (IE) and relative ionization efficiencies (RIEs). Pure ammonium nitrate (NH₄NO₃)
161 particles (size selected by 300 nm) are used for the calibration of the instrument, because
162 NH₄NO₃ vaporizes with 100% efficiency (Ng et al., 2011a). The RIEs values usually used in
163 Aerosol Mass Spectrometer (AMS) ambient concentration calculations (Canagaratna et al.,
164 2007) are the default values of organics (1.4), nitrate (1.1), sulfate (1.2), and chloride (1.3) in
165 this study. Moreover, the RIE value of ammonium is 7.04, and the response factor (RF) value
166 of nitrate is 3.96×10^{-11} in this study. In addition, the mass concentrations of ambient aerosol
167 need to be corrected for particle collection efficiency (CE) (Middlebrook et al., 2011). CE =
168 0.5 is found to be representative with data uncertainties generally within 20% (Canagaratna et
169 al., 2007; Middlebrook et al., 2011). The CE values observed in previous studies range from
170 0.43 to 1, due to (a) shape-related collection losses at the vaporizer from inefficient focusing
171 of non-spherical particles, (b) particle losses at the vaporizer because of bouncing of solid

172 particles before they are completely vaporized, and (c) particle losses in the aerodynamic
173 inlet as a function of particle diameter (Allan et al., 2004; Zhang et al., 2005b; Canagaratna et
174 al. 2007; Middlebrook et al., 2011). In this study, we selected the CE value for OA, nitrate,
175 sulfate, ammonium, and chloride, respectively, according to the equation $CE = \max(0.45,$
176 $0.0833 + 0.9167 \times \text{ANMF})$ (Middlebrook et al., 2011), in which ANMF is the mass fraction
177 of NH_4NO_3 measured by the ACSM.

178 The PMF method, combining PMF2 executables with the PMF Evaluation Tool (PET)
179 (Ulbrich et al., 2009), was applied to analyze OA datasets from the ACSM. More details of
180 procedure for the PMF model can be found in previous studies (Ulbrich et al., 2009; Zhang et
181 al., 2005a, 2011). Due to large interferences of internal standard of naphthalene at m/z 's 127
182 – 129, only $m/z < 120$ was used for PMF analysis (Sun et al., 2012, 2013). Based on the OA
183 dataset from the ACSM, the PMF analysis was performed for 1 to 7 factors. A summary of
184 the PMF results is presented in Figure S6 – S15. For the chosen number of factors, f_{peaks}
185 were varied in steps of 0.1 from –1 to 1 for the data of the summer and autumn harvest. Four
186 OA factors, i.e., hydrocarbon-like mixed with cooking OA (HOA + COA), fresh
187 biomass-burning OA (BBOA), oxidized BB-influenced OA (OOA-BB), and highly
188 oxygenated OA (OOA) were resolved in this study. The HOA + COA was considered as a
189 factor mixing with COA and traffic HOA in the 4-factor solution, while the “HOA + COA”
190 factor splits into factors with very similar time series in the five- to a seven-factor solution.
191 This means that the PMF analysis of the ACSM OA mass spectra has difficulties
192 distinguishing the COA from the traffic HOA in this study. Sun et al. (2010) and Sun et al.
193 (2012) also found a similar phenomenon for distinguishing COA from traffic HOA in a
194 Quadrupole AMS (Q-AMS) and an ACSM OA mass spectra using PMF analysis in Beijing.
195 For the 3-factor solution, BBOA might be mixed with OOA-BB, while the 4-factor solution
196 (which contained two BB-related BBOA factors, i.e., BBOA and OOA-BB) seemed to be

197 better (more details can be found in section 3.2) [than the other](#) solutions. The detailed lists of
198 explanation on the reasons for the selection of the 4-factor solution can be found in Table S4
199 – S5. In addition, the OA source apportionment for the two harvests will be further discussed
200 in section 3.2.

201

202 **2.2.3 Back-trajectory analysis**

203 Impacts of various source regions on the PM pollution during the harvest seasons have been
204 investigated using the HYbrid Single Particle Lagrangian Integrated Trajectory (HYSPLIT-4)
205 model developed by NOAA/ARL (Draxler and Rolph, 2003). Accordingly, 48 h
206 back-trajectories (BTs) at 500 m arrival height above ground level were calculated every 2 h
207 starting at China Standard Time (CST) using a Trajectory Statistics (TrajStat) software
208 developed by Wang et al. (2009b). In this study, the 48 h back-trajectories of air masses were
209 used for further analysis.

210

211 **3 Results and discussion**

212 **3.1 Meteorological factors and PM₁ components**

213 **3.1.1 Time series of meteorological factors and PM₁ components**

214 Figure 1 shows the time series of NR-PM₁ species and BC in the presence of different
215 meteorological conditions during the harvest seasons in urban Nanjing, i.e., WS, WD, RH, *T*,
216 and precipitation. During the summer harvest, the average values were $70.7 \pm 15.3\%$, $3.7 \pm$
217 1.7 m s^{-1} , and $23.4 \pm 4.1 \text{ }^\circ\text{C}$ for the ambient RH, WS, and *T*, respectively. In the autumn
218 harvest, the average values were $54.3 \pm 13.7 \%$, $2.6 \pm 1.4 \text{ m s}^{-1}$, and $18.1 \pm 3.6 \text{ }^\circ\text{C}$ for the
219 ambient RH, WS, and *T*, respectively. The frequency distribution of hourly averaged wind
220 direction and speed throughout the summer and autumn harvests are shown in Figure S2 (a –
221 b).

222 As shown in Figure S3, there is a strong correlation between the MET ONE PM₁
223 measured by MET ONE BAM-1020 and the PM₁ (= NR-PM₁ + BC) mass concentrations (r^2
224 = 0.88, *slope* = 1.11), indicating that the ambient submicron aerosols consisted mainly of the
225 NR-PM₁ and BC. Note that the mass concentration of BC in the PM₁ may be overestimated
226 due to the fact that the mass concentration of BC was measured by the 7-wavelength
227 aethalometer for PM_{2.5}. An overestimation was previously suggested by Huang et al. (2011).
228 The average PM₁ mass for the summer harvest is 38.5 $\mu\text{g m}^{-3}$ with hourly average ranging
229 from 3.6 to 270.6 $\mu\text{g m}^{-3}$, which is similar to that observed in the autumn harvest (42.3 μg
230 m^{-3}) with hourly average ranging 8.1 to 191.5 $\mu\text{g m}^{-3}$. Indeed, PM₁ consisted of OA (39%),
231 nitrate (23%), ammonium (16%), sulfate (12%), BC (8%), and chloride (1%) during the
232 summer harvest. During the autumn harvest, PM₁ was composed of OA (41%), nitrate (20%),
233 ammonium (14%), sulfate (11%), BC (13%), and chloride (1%). Table 1 presents a
234 comparison of the average composition of PM₁ between the summer harvest and autumn
235 harvest periods. The average bulk composition of PM₁ during the summer harvest shows
236 similar dominance of OA to the PM pollution during the autumn harvest, but lower mass
237 fractions for other species except nitrate. Overall, those species with the exception of BC also
238 show a similar contribution between the summer and autumn harvest to the PM₁ mass,
239 suggesting that the PM pollution could be affected by similar pollution sources for the two
240 harvests.

241 As shown in Figure 1, all aerosol species exhibited very dynamic variations in mass
242 concentrations due to the changes of source emissions, meteorology factors (such as WD, RH,
243 *T*, and planetary boundary layer height), photochemical reactions and regional transport (e.g.
244 the BB plumes). For example, the aerosol species dramatically reduced because of the quick
245 removal processes associated with heavy wet scavenging (e.g. 6 – 8 June) during the summer
246 harvest. However, the wet scavenging plays a minor role in changing aerosol loadings with

247 little precipitation during the autumn harvest. OA shows a significant dynamic variation in
248 mass concentrations during the harvest seasons (Fig. 1c), likely due to the changes of source
249 emissions (such as cooking, traffic and/or BB emissions). There are three sharp peaks during
250 the summer harvest (case 1) and autumn harvest (case 2 and case 3). The relationships
251 between the PM pollution, meteorology and chemical composition are presented in three case
252 events (Table S1). The case 1, at 21:00 – 22:00 on 10 June, with the highest PM₁ mass (253.1
253 $\mu\text{g m}^{-3}$) during the summer harvest is characterized by high loadings of K⁺, BBOA, OOA-BB,
254 chloride, and BC, indicating the significant impacts of agricultural burning from the
255 northwest of Nanjing (Fig. 1). Apart from the high loadings of BB-related components, such
256 as BBOA, OOA-BB, and K⁺ seen in the case 2 and case 3 periods, local source-related
257 components, e.g., HOA + COA and BC, also present high concentrations. This suggests that
258 both local primary sources emission and regional BB plumes dominate the PM pollution
259 during the case 2 and case 3 periods. Therefore, those findings indicate that indeed BB
260 contributes significantly in the area during the specific time period.

261

262 **3.1.2 Diurnal variations of meteorological factors and PM₁ components**

263 Figure 2 depicts the diurnal variations of the meteorological factors, i.e., RH, *T*, and WS, and
264 PM₁ species (including OA, nitrate, sulfate, ammonium, chloride, and BC). Generally, the
265 diurnal variations of the meteorological parameters and PM₁ species are similar during the
266 summer and autumn harvest. However, the ambient RH and *T* during summer harvest were
267 higher than those during autumn harvest. OA obviously exhibits three peaks occurring
268 between 6:00 – 8:00, 11:00 – 14:00, and 19:00 – 22:00, which is in agreement with the
269 contributions of pollution sources, e.g., traffic, cooking and/or BB (Allan et al., 2010; Huang
270 et al., 2012; Sun et al., 2012; Crippa et al., 2013). More details of the diurnal variations of the
271 OA components will be presented in section 3.2.

272 Sulfate does not show any significant diurnal trend during both summer and autumn
273 harvest, and shows a similar concentration during the two harvests. This means the
274 non-volatile character and regional pollution of sulfate in the YRD region during the summer
275 and autumn harvest. Similar diurnal trend of sulfate was also found by Huang et al. (2012) in
276 the eastern YRD region. Nitrate presents in a higher fraction of the total PM₁ compared with
277 sulfate, yet with lower concentrations in the afternoon and higher concentrations in the
278 evening during the harvests. Similarly, nitrate also shows a similar concentration for the two
279 harvests during the whole day. In addition, chloride shows a similar diurnal cycle with nitrate
280 during the two harvest seasons. This is in accordance with the volatile and gas-particle
281 partitioning properties of ammonium nitrate and ammonium chloride dependent on ambient *T*
282 and RH (Lanz et al., 2007; Sun et al., 2011b, 2012). This also reflects that the photochemical
283 production of HNO₃ cannot compensate for the evaporative loss at the relatively high *T*
284 conditions during the two harvests, which is similar to previous results observed by Huang et
285 al. (2012) in the eastern YRD region and Sun et al. (2012) in Beijing. Furthermore, the higher
286 boundary layer may dilute their loadings during the daytime, and then influence their diurnal
287 cycles (Sun et al., 2012). Chloride is mainly ammonium chloride (NH₄Cl) and/or organic
288 chlorine-containing species (Huffman et al., 2009; Huang et al., 2012; Sun et al., 2012).
289 During the harvest seasons, the evening high values of nitrate and chloride might be affected
290 by the BB emissions and/or formed via gas-phase and aqueous-phase oxidations.

291 BC shows a classic diurnal variation with higher loadings appearing in early morning and
292 during nighttime, which is consistent with traffic rush hours in early morning (07:00 – 08:00)
293 and during nighttime (20:00 – 21:00). As in previous studies, atmospheric BC is strongly
294 associated with combustion emissions (including traffic and BB sources emissions),
295 particular for BB periods (Sandradewi et al., 2008; Liu et al., 2011, 2014; Crippa et al., 2013).
296 Therefore, the reason for the peak values of BC during the nighttime may be also caused by

297 the BB emissions during the harvest seasons, apart from the effect of traffic source on the BC
298 loadings. The lower concentrations of BC in the afternoon can be associated with the dilution
299 effects of higher planetary boundary layer and reduced traffic emissions.

300

301 **3.2 Organic source apportionment**

302 Four OA factors (i.e. HOA + COA, BBOA, OOA-BB, and OOA) were identified, as
303 illustrated in Figure 3 and Figure 4. The mean mass concentrations of HOA + COA, BBOA,
304 OOA-BB and OOA during the harvest seasons are presented in Table 1. HOA + COA, BBOA,
305 OOA-BB, and OOA accounted on average for 15% (28%), 7% (7%), 29% (33%) and 49%
306 (32%) of the total OA mass concentrations during the summer (autumn) harvest, respectively.

307

308 **3.2.1 Hydrocarbon-like and cooking-emission related OA (HOA + COA)**

309 The prominent hydrocarbon ion series of $C_nH_{2n+1}^+$ and $C_nH_{2n-1}^+$ (e.g. 27, 29, 41, 43, 55, 57...)
310 obtained from the mass spectrum were characterized as components of HOA (Zhang et al.,
311 2005a, 2011; Mohr et al. 2009; Allan et al., 2010). As reported in previous studies, m/z 57
312 ($C_3H_5O^+$ and/or $C_4H_9^+$) and m/z 55 ($C_3H_3O^+$ and/or $C_4H_7^+$) are commonly considered as
313 tracers for the primary organic emissions of combustion sources in urban areas, including
314 COA and HOA (Zhang et al., 2005a; Ng et al., 2010, 2011b; He et al., 2010; Sun et al., 2012,
315 2013; Hu et al., 2013). It is found that there is no significant difference in the mass spectrum
316 between the summer harvest and the autumn harvest (Fig. 3a). Compared with traffic-like OA
317 (Liu et al., 2011; Crippa et al., 2013), the mass spectrum obtained in the present study shows
318 a higher m/z 55/57 ratio. Previous studies indicated that high m/z 55/57 together with a unique
319 diurnal variation can be used as a diagnostics for the presence of COA (Mohr et al., 2009;
320 Allan et al., 2010; Sun et al., 2012). The mass spectrum of HOA in this study is characterized
321 by more abundant ions, i.e., m/z 41 (mainly $C_3H_5^+$), m/z 55 (mainly $C_4H_7^+$) and m/z 57 (Fig.

322 3a), which is similar to the characteristics of COA mass spectrum measured by He et al.
323 (2010). As shown in Figure 3, the diurnal variation of HOA + COA shows two pronounced
324 peaks corresponding to noon (a weak peak) and evening traffic/cooking activities (a strong
325 peak). Hence, HOA + COA in this study refers to the sum of traffic-related HOA and COA.
326 Similarly, Sun et al. (2010) and Sun et al. (2012) also found that HOA species in urban
327 ambient were influenced by both traffic and cooking-like emissions.

328

329 **3.2.2 Fresh biomass burning OA (BBOA)**

330 As shown in Figure 3b, the mass spectrum of BBOA extracted in this study shows a
331 prominent peak of m/z 60 which is a well-known tracer ion for BB emissions (Alfarra et al.,
332 2007; Aiken et al., 2009; Cubison et al., 2011; Huang et al., 2011; Liu et al., 2011).
333 Levoglucosan was shown to contribute to m/z 60 and was found in large amounts in urban,
334 suburban, and rural background atmosphere during BB periods (Maenhaut et al., 2012). In
335 addition, the BBOA is also characterized by higher peaks at masses m/z 27, 29, 41, 43, 55, 57,
336 77 and 91 that are indicative of freshly emitted organic aerosol, because fresh m/z 43 ... m/z
337 57 can be also from BB-related emissions (Aiken et al., 2009; Heringa et al., 2011;
338 Bougiatioti et al., 2014). For example, primary BBOA (P-BBOA) has a significant
339 contribution from a non-oxygenated ion $C_3H_7^+$ at m/z 43, but not from an oxygenated ion
340 $C_2H_3O^+$ (m/z 43) in smog chamber experiments by Heringa et al. (2011). The BBOA
341 spectrum profiles with the lack of m/z 44 signal (CO_2^+) during the summer and autumn
342 harvest show high correlation ($r^2 = 0.82$ and $r^2 = 0.87$) with a result in Paris (Crippa et al.,
343 2013). Moreover, the spectrum of BBOA in this study is qualitatively similar to published BB
344 spectra from the fresh BB smoke in a smog chamber (Grieshop et al., 2009). These findings
345 suggest that this factor can be related to BBOA with low atmospheric oxidants, and thus this
346 factor might this factor might be associated with fresh/primary BBOA during the harvests.

347 Using soluble K^+ as a tracer for BB has also been reported by previous analyses of BB
348 campaign data (Gilardoni et al., 2009; Aiken et al., 2010; Du et al., 2011; Crippa et al., 2013).
349 The time series of BBOA along with K^+ measured by MARGA is shown in Figure 4b. BBOA
350 is strongly correlated with K^+ ($r^2 = 0.95$ and $r^2 = 0.78$) during the summer and autumn
351 harvest respectively (Fig. 5a), suggesting that BBOA and K^+ were from the same source. In
352 addition, the diurnal variation of BBOA shows a pronounced peak at the nighttime (Fig. 3),
353 which is consistent with the effects of the BB emissions (Fig. 3). This means that BBOA
354 contributes to primary organic aerosol (POA) during the nighttime mainly. This finding is
355 also consistent with the habit of the farmers in the YRD region, namely that they usually
356 harvest wheat or rice in the daytime and burn off straw in the nighttime during the harvest
357 seasons each year. In addition, chloride correlates well with BBOA ($r^2 = 0.61$ and $r^2 = 0.66$)
358 and K^+ ($r^2 = 0.60$ and $r^2 = 0.64$) during the harvest seasons (Figure S5). This suggests that
359 chloride was mainly from the BB emissions and might be in the form of KCl during the BB
360 periods.

361

362 **3.2.3 Oxygenated OA (OOA) and oxidized BB-influenced OA (OOA-BB)**

363 The mass spectrum of both OOA components (Fig. 3c and d) was characterized by the
364 prominent $C_xH_yO_z^+$ fragments, which has been denoted previously found in many AMS
365 studies (Zhang et al., 2005a; Lanz et al., 2007; Sun et al., 2010; Crippa et al., 2013). The
366 mass spectra of OOA by the prominent peak of m/z 44 (mainly CO_2^+) (22.9% and 25.5% of
367 the total OOA signal respectively) during the summer and autumn harvest are strongly
368 consistent with more oxidized OOA component determined ($r^2 = 0.91$ and $r^2 = 0.89$, Fig. 3d)
369 in BB-period in Paris (Crippa et al., 2013) and OOA components resolved at other urban sites
370 (Lanz et al., 2007; Ulbrich et al., 2009).

371 In Figure 4d the time series of OOA is compared with the sulfate mass loadings. A

372 correlation was observed between time series of OOA and sulfate mass loadings ($r^2 = 0.60$
373 and $r^2 = 0.46$, Fig. 6) during the summer and autumn harvests, respectively. Previous studies
374 performed at various sites also showed that these two species were secondary with
375 low-volatility property in the atmosphere (Zhang et al., 2005a; Lanz et al., 2007; Ulbrich et
376 al., 2009; Sun et al., 2011a; Huang et al., 2012). Overall, the diurnal pattern of OOA shows
377 relatively stable trend throughout the whole day (Fig. 3). OOA often remains at a high
378 concentration across several days until a change of air mass occurs, which shows a regional
379 production (Sun et al., 2012, 2013). This may be a main reason causing the relatively stable
380 trend through the whole day in this study. Nevertheless, OOA shows a slight increase at
381 around 12:00 – 15:00, suggesting that more oxidized OOA might be formed by
382 photochemical processing. OOA also exhibits higher loadings during the nighttime, probably
383 caused by the aging of BB plumes, in which BB emissions will be further oxidized and begin
384 to transition into OOA (Jimenez et al., 2009, DeCarlo et al., 2010). The uniform distribution
385 of its concentrations is almost in association with all kinds of WD during the summer and
386 autumn harvest respectively (Figure S4). This is a good evidence for explaining the regional
387 pollution of OOA in the YRD region during the harvest seasons.

388 Additionally, an oxygenated factor with the high degree of oxygenation during the
389 summer and autumn harvest (m/z 44, 18.2% and 14.5% of the total factor signal respectively)
390 in its mass spectrum has been resolved and identified as oxidized BB-influenced OA
391 (OOA-BB, Fig. 3c). The mass spectra of OOA-BB are characterized by both the oxidized
392 ions (m/z 18, 29, 43 and 44) and the typical marker of BB (m/z 60) during the summer and
393 autumn harvest, which correlates well with those of BB-emission related OOA
394 (OOA₂-BBOA) ($r^2 = 0.85$ and $r^2=0.86$) during BB periods at an urban site in Paris (Crippa et
395 al., 2013). It is also highly similar to the mass spectrum of the aged BBOA identified by
396 DeCarlo et al. (2010) for airborne measurements during the MILAGRO campaign, and very

397 in agreement with the aged BBOA from a BB experiment in a chamber study by Heringa et al.
398 (2011). In addition, the mass spectrum of OOA-BB shows more oxygenated degree,
399 compared to mass spectrum of fresh/primary BBOA from PMF analysis in the atmosphere
400 and from laboratory open wood burning (Aiken et al., 2009) and from BBOA in this study.
401 The OOA-BB spectrum in this study is also very similar to the spectrum of the aged OA
402 produced from aged biomass smoke in a smog chamber (Grieshop et al., 2009). OOA-BB
403 presents a pronounced diurnal cycle with the highest concentration in the evening and early
404 morning during the harvests (Fig. 3), which is very consistent with the diurnal variations of
405 BBOA. This means that the OOA-BB [production from open BB](#) is rapid in short timescales
406 with the high RH and low T conditions in the nighttime. OOA-BB also shows relatively low
407 loadings in the daytime, due to the dilution effects by enhanced mixing in the planetary
408 boundary layer and the evaporative loss of semi-volatile components.

409 As shown in Figure 4c, the OOA-BB time series strongly correlates with K^+ and $\Delta m/z$
410 60 ($= m/z\ 60 - 0.26\% \times OA$, in which applied metric of background $f_{60} = 0.26\%$ of OA will
411 be discussed in section 3.4) during the summer and autumn harvest, supporting the BB
412 influence. In addition, the sum of BBOA and OOA-BB also shows high correlation with K^+
413 and $\Delta m/z\ 60$ for the two harvests (Fig. 5a – b). This suggests that OOA-BB represents an
414 atmospheric mixture of BBOA and OOA, which is similar to a recent HR-ToF-AMS study by
415 Crippa et al. (2013). It is interesting that OOA-BB correlates well with nitrate ($r^2 = 0.30$ and
416 $r^2 = 0.54$), yet shows lower correlation with sulfate ($r^2 = 0.16$ and $r^2 = 0.30$) for the summer
417 and autumn harvest respectively (Fig. 6). Also, the time series of OOA-BB shows a similar
418 trend as chloride during the two harvest seasons (Fig. 4c). This implies an indication of the
419 semi-volatile character of OOA-BB, which is consistent with the results from a recent field
420 study in the eastern Mediterranean (Bougiatioti et al., 2014) and some laboratory chamber
421 studies (Lipsky and Robinson, 2006; Robinson et al., 2007; Yee et al., 2013). Particularly, this

422 also means that aged biomass burning OA (OOA-BB) may be significantly mixed with nitrate
423 in the BB plumes. Healy et al. (2013) also found a similar result in Paris using single-particle
424 mass spectrometer (SP-AMS) and HR-ToF-AMS measurements.

425

426 **3.3 Effects of Chemical components on PM pollution**

427 Figure 7 presents the average contributions of PM₁ species and OA components during the
428 summer and autumn harvest, respectively. It is also compared with other sites, including
429 megacities (Mexico City, Paris, Beijing, and Shanghai), and suburban/remote areas (Crete,
430 Jiaxing, and Pearl River Delta) (Aiken et al., 2009; Crippa et al., 2013; Huang et al., 2012,
431 2013; Sun et al., 2012; Bougiatioti et al., 2014). Using the relative contribution of the sum of
432 BBOA and OOA-BB to OA, the harvest season was separated into 3 time periods, i.e., low
433 BB (L-BB, 28% and 29%) period, medium BB (M-BB, 49% and 38%) period, and high BB
434 (H-BB, 93% and 50%) period, during the summer and autumn harvest respectively. We also
435 include averages of some meteorological parameters (i.e. RH, *T*, WS, and WD) for the
436 reference, and these averages are shown in Table S2. Compared with other sites including
437 Mexico City, Paris, Crete, Jiaxing, and Pearl River Delta (Fig. 7), the BB source shows the
438 largest contribution to aerosol pollution during the H-BB both in the summer and autumn
439 harvest in urban Nanjing. In addition, in the absence of BB source the sum of OOA and
440 OOA-BB shows a higher fraction of total OA mass during the harvests in urban Nanjing in
441 comparison with Beijing and Shanghai in China (Fig. 7). This means that the BB source
442 significantly contributes to the SOA pollution in urban Nanjing during harvest seasons.

443 As shown in Figure 7, OA is important in PM pollution in the summer and autumn
444 harvest (39% and 41%). Furthermore, the average fraction of BBOA to OA during the
445 summer harvest (7%) is highly consistent with that in the autumn (7%), while BC shows a
446 higher fraction during the autumn harvest (12%) than that in the summer harvest (8%). This

447 is also corresponding to the fraction of HOA + COA, which shows a higher contribution
448 during the autumn harvest (28%) than that in the summer harvest (15%). The different
449 boundary layer height and primary sources emission influences on primary pollutants
450 (including BC, HOA and COA) may be all potential causes of such seasonal differences. On
451 average, the total oxidized fraction of OA (including OOA and OOA-BB) accounts for more
452 than 60% (78% for summer and 65% for autumn harvest), which indicates that regional OOA
453 plays an important role in PM pollution in urban Nanjing during the harvest seasons. As a
454 comparison, OOA-BB shows a higher fraction to OA in H-BB period than in L-BB period.
455 The fraction of OOA-BB to OA is higher than the fraction of BBOA during the harvest
456 seasons, even in the H-BB period. These findings indicate that “aged” BBOA plays a more
457 significant role in PM pollution than BBOA in the BB plumes, particularly in the H-BB
458 period. This is consistent with recent studies (Grieshop et al., 2009; Heringa et al., 2011;
459 Lathem et al., 2013; Yee et al., 2013; Bougiatioti et al., 2014) indicating that the fresh BB
460 emission OA can be rapidly surpassed by SOA formation within a few hours after its
461 emission.

462 The secondary inorganic aerosols (including sulfate, nitrate, and ammonium) can be
463 seen in lower fraction in the H-BB period than in the L-BB period. However, the mass
464 concentrations of sulfate, nitrate and ammonium are higher in the H-BB period than in the
465 L-BB period (Table S2) respectively. Therefore, these findings indicate [that the BB source](#)
466 contributes more to OA than secondary inorganic components. It is interesting that the
467 contribution of nitrate to PM₁ is higher than the contribution of sulfate in the H-BB periods
468 during the two harvest seasons. For example, the average contribution of nitrate to PM₁ is
469 ~18% in the H-BB periods, which is almost twice higher than that of sulfate. However, the
470 contribution of nitrate to PM₁ is very similar to the sulfate contribution in the L-BB periods.
471 All of those indicate the BB is a much more important source of nitrate, compared to sulfate.

472 Similar results have been observed by Crippa et al. (2013), Healy et al. (2013) and
473 Bougiatioti et al. (2014) during open BB periods.

474 Figure 8 presents the mass fractions of PM₁ species and OA components as a function of
475 total PM₁ mass loadings, as well as the probability density of total PM₁ mass loadings during
476 the summer and autumn harvest respectively. Overall, the total OA fraction increases from
477 about ~15% to 40% and from ~30% to 45% as a function of the PM₁ loadings during summer
478 and autumn, respectively. Indeed, OOA-BB and BBOA show a significant increase as a
479 function of the PM₁ loadings respectively during the harvest seasons. The contribution of
480 OOA-BB to PM₁ increases from ~3% (~5%) to 33% (26%) during the summer (autumn)
481 harvest. And the contribution of BBOA increases from ~2% (~4%) to 8% (8%). The results
482 highlight the contribution of OOA-BB arising from BB emissions to PM pollution in the
483 harvests. During the summer harvest, the HOA + COA and BC mass fractions display a slight
484 decrease, suggesting that local primary sources play an important in the low PM pollution
485 period. In addition, the nitrate and sulfate contributions show a slight increase and decrease
486 respectively, indicating additional production of nitrate mass during high PM episodes. Note
487 that the mass fraction of OOA shows a slight decrease with the increasing of total PM₁
488 loadings during the autumn harvest. This suggests that OOA mainly contributes to the low
489 PM pollution, and OOA-BB mainly contributes to the high PM pollution. However, the
490 contribution of HOA + COA, BC, and the secondary inorganic species to the total PM₁
491 loadings did not show clear PM-mass loading dependency, which indicates that the high PM
492 pollution during the autumn harvest may be caused by the synergistic effects of all pollutants.

493

494 **3.4 Estimation of BBOA directly from a tracer ($\Delta m/z$ 60)**

495 The BBOA mass loadings during the harvest seasons were estimated a posteriori using a
496 simple method. As described in previous studies, the parameter f_{60} , fraction of m/z 60 in total

497 OA, is considered as a marker of fresh/primary BBOA (Alfarra et al., 2007; DeCarlo et al.,
498 2008; Aiken et al., 2009; Cubison et al., 2011). To estimate the real value of the BBOA
499 loadings, the background fraction of f_{60} ($0.26 \pm 0.1\%$) during little/negligible BB-influence
500 periods (non-BB periods) was determined (Fig. 9). Aiken et al. (2009) and Cubison et al.
501 (2011) also obtained a similar background level of f_{60} ($0.3 \pm 0.06\%$) for an urban city in
502 Mexico Therefore, the levoglucosan-like species in ambient BB plumes was estimated by Δ
503 m/z 60 ($\Delta m/z$ 60 = m/z 60 – background value of $f_{60} \times OA$). As shown in Figure 5b, the
504 strong correlations ($r^2 = 0.95$, $r^2 = 0.98$, and $r^2 = 0.97$) between the BBOA and $\Delta m/z$ 60 with
505 the similar slopes, i.e., 16.3 for summer, 14.6 for autumn, and 15.1 for the total harvest
506 seasons, were observed. The OOA-BB mass loadings also show the high correlations with Δ
507 m/z 60 ($r^2 = 0.95$ and $r^2 = 0.97$), but with very different slopes (74.8 and 64.4) during the
508 summer and autumn harvest respectively (Fig. 5b). Aiken et al. (2009) also found that BBOA
509 strongly correlated with $\Delta m/z$ 60 mass loadings ($r^2 = 0.91$, $Slope = 34$) during the
510 BB/wood-smoke periods in Mexico City. Furthermore, Lee et al. (2010) obtained a strong
511 relationship between BBOA and m/z 60 mass loadings ($r^2 = 0.92$, $Slope = 34.5$) through a
512 wildland fuels fire experiment in the lab. Thus, we reconstructed the time series of BBOA to
513 compare the relationship between the extracted BBOA by PMF model (PMF BBOA) and the
514 estimated BBOA. As shown in Figure S16, an excellent agreement is observed between the
515 identified and reconstructed BBOA concentrations during the total harvest seasons ($r^2 = 0.97$).
516 Therefore, the BBOA component during the BB periods in urban Nanjing of the YRD region
517 can be estimated with the equation of $BBOA = 15.1 \times (m/z$ 60 – $0.26\% \times OA)$ for the harvest
518 seasons.

519

520 **3.5 Evaluation of OA**

521 To further investigate the probable importance of the aging and/or mixing processes of

522 BB plumes, the total BB-related OA (BBOA + OOA-BB) to ΔCO ratio as a function of the
523 f_{44} during the summer and autumn harvest respectively is shown in Figure 10. The CO
524 background is determined as $14.9 \mu\text{g m}^{-3}$ for summer harvest and $17.9 \mu\text{g m}^{-3}$ for autumn
525 harvest, respectively, based on an average of the lowest 5% CO during two plumes
526 (Takegawa et al., 2006). The ratio of BBOA + OOA-BB to ΔCO can remove the effect of
527 dilution in the atmosphere (de Gouw 2005; Dunlea et al., 2009; DeCarlo et al., 2008, 2010).
528 As discussed in de Gouw et al. (2005), Aiken et al. (2008), Jimenez et al. (2009), and Ng et al.
529 (2010), the f_{44} can be considered as indicator of atmospheric aging due to photochemical
530 aging processes leading to the increasing of f_{44} in the atmosphere. Overall, the (BBOA +
531 OOA-BB) / ΔCO ratio shows an obvious reduction with increasing of f_{44} values during the
532 summer and autumn harvest respectively, in the absence of traffic and cooking-like plumes.
533 This is likely due to a synergistic effect of the rapid formation of OOA from BB plumes and
534 the mixing of BBOA with regional OOA and/or CO. Similar results have been found by
535 DeCarlo et al. (2010), from aircraft measurements during MILAGRO in Mexico City and the
536 Central Mexican Plateau.

537 Figure 11a depicts the evolution process of OA with the f_{44} vs. f_{43} space during two
538 harvest seasons. The BBOA and HOA + COA show similar low oxidative properties with
539 varying f_{43} , which are located at the left-bottom of the triangular region during the summer
540 and autumn harvest, respectively. With the aging process in the atmosphere, OA clusters
541 within a well-defined triangular region and shows more similar oxidative properties to
542 OOA-BB and/or OOA (Fig. 11a). This implies that OOA-BB and/or BBOA might be further
543 oxidized, and might be transformed into highly oxidized OOA.

544 Furthermore, the formation and transformation of primary and secondary BBOA during
545 BB periods can be described by f_{44} vs. f_{60} plot (Cubison et al., 2011). In the f_{44} vs. f_{60} space of
546 Figure 11b, OA shows a trend toward higher f_{44} and lower f_{60} values with the aging of BB

547 plumes, appearing into the low-volatility OOA (LV-OOA) range. This is very consistent with
548 previous reports in aircraft and laboratory studies (Cubison et al., 2011) with a similar trend.
549 In a smog chamber experiment, Grieshop et al. (2009) also found that the relative
550 contribution at m/z 44 and m/z 60 rapidly increases and decreases, respectively during aging
551 process, which presents the characteristics of fresh and aged BBOA.

552

553 **3.6 Impacts of various source regions on the PM pollution**

554 Figure 12 presents the BTs clusters of air masses at 500 m arrival height above ground
555 level at intervals of two hours (i.e. 00:00, 02:00, 04:00, ..., 22:00) starting at CST using the
556 HYSPLIT model (Draxler and Rolph, 2003) in Nanjing (118°46'N, 32°05'E). The
557 corresponding BTs can be broadly classified into four principal clusters of air masses based
558 on the spatial distributions during the summer and autumn harvests, respectively, i.e.,
559 northeasterly (NE) back-trajectories (BTs), easterly marine (EM) BTs, southeasterly marine
560 (SEM) BTs, and southwesterly continental (SWC) for the summer harvest; northerly
561 continental (NC) BTs, northeasterly marine (NEM) BTs, easterly marine (EM) BTs and
562 southerly continental (SC) for the autumn harvest. The air masses in Nanjing in this study
563 were mainly from the SEM BTs (accounting for 57.4% of all the BTs) during the summer
564 harvest, while predominantly from the NC and EM BTs (at frequencies of 43.8% and 24%,
565 respectively) during the autumn harvest (Fig. 12 and Table S3).

566 The average PM_{10} loadings are the highest ($71.3 \mu g m^{-3}$) for the WC BTs, which is
567 almost twice higher than that of the lowest ($24.4 \mu g m^{-3}$) for the EM BTs during the summer
568 harvest. This suggests that the long-range transported pollutants from southwestern areas can
569 cause the high PM pollution in the YRD region during the summer harvest. Similarly, the
570 highest average concentration of PM_{10} ($80.9 \mu g m^{-3}$) is associated with the continental-related
571 air masses during the autumn harvest. Therefore, source regions related to the fire locations

572 (Figure S1) are of utmost importance to the high air pollution in the YRD region during the
573 harvest seasons.

574 The PM₁ chemical compositions show also significantly different fraction among the
575 four clusters during the summer and autumn harvest respectively, which might be associated
576 with the different source regions of air pollution. The lowest PM₁ loadings are associated
577 with the EM BTs, but with the high contribution of HOA + COA during the summer harvest
578 (Fig. 12a). This suggests that the local sources play a key controller of aerosol pollution
579 during relatively clean periods in the summer harvest. For the NE BTs, the OOA, nitrate, and
580 sulfate provide high fractions of the total PM₁ mass, suggesting that regional pollution plays a
581 key role in controlling the PM pollution. With regards to the marine-related air masses, PM₁
582 loadings associated with the NEM and NE BTs are higher in the summer harvest than in the
583 autumn harvest (Fig. 12b), which may be due to the fact that high local POA contributes to
584 the PM pollution. This suggests that local sources [play a more](#) important role in the aerosol
585 pollution in the summer harvest than in the autumn harvest. Compared with other clusters
586 during the autumn harvest, the BB-related components (e.g. BBOA, OOA-BB and chloride)
587 contribute the highest fractions to the PM₁ mass in air masses originated from the SC BTs,
588 indicating that BB plumes can contribute to the highest heaviest PM pollution during the
589 autumn harvest. Apart from the high contributions of nitrate and OOA, HOA + COA also
590 accounted a higher fraction to PM₁ mass in the NEM and EM BTs than in other clusters
591 during the autumn harvest. In addition, the PM₁ components show the lowest concentrations
592 for the NC BTs, compared to the other clusters during the autumn harvest. When removing
593 the mass concentrations of BB related OA (BBOA and OOA-BB), the mean concentration of
594 PM₁ (31.6 $\mu\text{g m}^{-3}$) for the NC BTs is corresponding to a result (28.7 $\mu\text{g m}^{-3}$) for a similar
595 cluster during a non-BB period (Huang et al., 2012).

596 **4 Conclusions**

597 The characteristics, sources and evolution of atmospheric PM₁ species in urban Nanjing, the
598 YRD region of China were investigated using an Aerodyne ACSM during the two harvest
599 seasons, namely the summer wheat harvest (June 1 to 15, 2013) and the autumn rice harvest
600 (October 15 to 30, 2013). The PM₁ species show a similar contribution, which on average
601 account for 39% (41%) OA, 23% (20%) nitrate, 16% (14%) ammonium, 12% (11%) sulfate,
602 8% (13%) BC, and 1% (1%) chloride during the summer (autumn) harvest. Secondary
603 inorganic species, i.e., nitrate, sulfate and ammonium, show highly similar diurnal patterns
604 between the summer and autumn harvest, meaning its similar chemical processing and
605 physical processes (e.g. gas-particle partitioning). In particular, OA, chloride and BC present
606 higher concentrations in the diurnal cycles during the autumn harvest than during the summer
607 harvest, due to larger impacts of BB and/or local primary emissions during the autumn
608 harvest.

609 PMF analysis was performed on the ACSM OA mass spectra to investigate organic
610 source apportionment during the two harvests. Four OA components were resolved including
611 two POA factors associated with traffic and cooking (HOA + COA) and biomass burning OA
612 (BBOA) emissions and two secondary factors associated with regional and highly oxidized
613 OOA and less oxidized BB-like OA (OOA-BB). Apart from HOA + COA, BBOA and
614 OOA-BB also present pronounced diurnal cycles during the harvests, with the highest
615 concentrations occurring at night due to the nighttime BB plumes over urban Nanjing. This
616 suggests that BBOA components may be quickly oxidized to OOA-BB during the nighttime
617 with the high RH and low *T* conditions. The diurnal profiles of OOA are similar to that of
618 sulfate with relatively flat variations, reflecting their regional origin. OA was dominated by
619 secondary organics (OOA and OOA-BB) with the fraction more than 60% to total OA mass.
620 POA shows a lower contribution to OA during the summer (autumn) harvest, traffic and

621 cooking 15% (28%) and BB 7% (7%) emissions. The background level of f_{60} ($0.26 \pm 0.1\%$)
622 was determined using the f_{44} vs. f_{60} space during the non-BB periods (in July). Thus, we
623 suggest a simpler method for estimating the fresh BBOA loadings based on the equation of
624 $BBOA = 15.1 \times (m/z\ 60 - 0.26\% \times OA)$ during the harvests. The $(BBOA + OOA-BB) / \Delta CO$
625 ratios decrease with the increasing of the f_{44} , suggesting that BBOA components may be
626 oxidized to more aged and less volatile OOA, e.g., LV-OOA during the aging process. Air
627 mass trajectory analysis indicates that the high PM pollution is mainly contributed by nitrate,
628 BBOA, and OOA-BB, which is associated with air masses originated from the western
629 (summer harvest) and southern (autumn harvest) areas.

630

631 *Acknowledgements*

632 This work was funded by the Natural Science Key Research of Jiangsu Province High
633 Education (11KJA170002), the Foundation Research Project of Jiangsu Province
634 (BK2012884, BK20140987), the Project Funded by the Jiangsu Province Science &
635 Technology Support Program (BE2012771), the Environmental Monitoring Scientific
636 Research Foundation of Jiangsu Province (1016), and the National Natural Science
637 Foundation of China (21407080). We are very grateful for the help and support from Dr.
638 Douglas R. Worsnop and Dr. John T. Jayne (Aerodyne Research Inc.) in the ACSM
639 measurements. We also would like to thank Dr. P. Chen (Handix LLC), and Dr. W. Li (South
640 Coast Air Quality Management District) for their constructive suggestions in improving the
641 contents. We thank the reviewers for their valuable comments on the manuscript.

642

643 **References**

644 Aiken, A. C., Decarlo, P. F., Kroll, J. H., Worsnop, D. R., Huffman, J. A., Docherty, K. S.,

645 Ulbrich, I. M., Mohr, C., Kimmel, J. R., Sueper, D., Sun, Y., Zhang, Q., Trimborn, A.,
646 Northway, M., Ziemann, P. J., Canagaratna, M. R., Onasch, T. B., Alfarra, M. R., Prevot,
647 A. S. H., Dommen, J., Duplissy, J., Metzger, A., Baltensperger, U., and Jimenez, J. L.:
648 O/C and OM/OC ratios of primary, secondary, and ambient organic aerosols with
649 high-resolution time-of-flight aerosol mass spectrometry, *Environ. Sci. Technol.*, 42,
650 4478–4485, 2008.

651 Aiken, A. C., Salcedo, D., Cubison, M. J., Huffman, J. A., DeCarlo, P. F., Ulbrich, I. M.,
652 Docherty, K. S., Sueper, D., Kimmel, J. R., Worsnop, D. R., Trimborn, A., Northway, M.,
653 Stone, E. A., Schauer, J. J., Volkamer, R. M., Fortner, E., de Foy, B., Wang, J., Laskin, A.,
654 Shutthanandan, V., Zheng, J., Zhang, R., Gaffney, J., Marley, N. A., Paredes-Miranda, G.,
655 Arnott, W. P., Molina, L. T., Sosa, G., and Jimenez, J. L.: Mexico City aerosol analysis
656 during MILAGRO using high resolution aerosol mass spectrometry at the urban
657 supersite (T0) – Part 1: Fine particle composition and organic source apportionment,
658 *Atmos. Chem. Phys.*, 9, 6633-6653, doi:10.5194/acp-9-6633-2009, 2009.

659 Aiken, A. C., de Foy, B., Wiedinmyer, C., DeCarlo, P. F., Ulbrich, I. M., Wehrli, M. N.,
660 Szidat, S., Prévôt, A. S. H., Noda, J., Wacker, L., Volkamer, R., Fortner, E., Wang, J.,
661 Laskin, A., Shutthanandan, V., Zheng, J., Zhang, R., Paredes-Miranda, G., Arnott, W. P.,
662 Molina, L. T., Sosa, G., Querol, X., and Jimenez, J. L.: Mexico city aerosol analysis
663 during MILAGRO using high resolution aerosol mass spectrometry at the urban
664 supersite (T0) - Part 2: Analysis of the biomass burning contribution and the non-fossil
665 carbon fraction, *Atmos. Chem. Phys.*, 10, 5315-5341, doi:10.5194/acp-10-5315-2010,
666 2010.

667 Alfarra, M. R., Prévôt, A. S. H., Szidat, S., Sandradewi, J., Weimer, S., Schreiber, D., Mohr,
668 M., and Baltensperger, U.: Identification of the mass spectral signature of organic
669 aerosols from wood burning emissions, *Environ. Sci Technol.*, 41, 5770-5777, 2007.

670 Allan, J. D., Bower, K. N., Coe, H., Boudries, H., Jayne, J. T., Canagaratna, M. R., Millet, D.
671 B., Goldstein, A. H., Quinn, P. K., Weber, R. J., W. D. R.: Submicron aerosol
672 composition at Trinidad Head, California, during ITCT 2K2: Its relationship with gas
673 phase volatile organic carbon and assessment of instrument performance, *J. Geophys.*
674 *Res.*, 109: D23S24, 2004.

675 Allan, J. D., Williams, P. I., Morgan, W. T., Martin, C. L., Flynn, M. J., Lee, J., Nemitz, E.,
676 Phillips, G. J., Gallagher, M. W., and Coe, H.: Contributions from transport, solid fuel
677 burning and cooking to primary organic aerosols in two UK cities, *Atmos. Chem. Phys.*,
678 10, 647-668, doi:10.5194/acp-10-647-2010, 2010.

679 Andreae, M. O., and Merlet, P.: Emission of trace gases and aerosols from biomass burning,
680 *Global Biogeochem. Cycles*, 15, 955-966, 2001.

681 Bougiatioti, A., Stavroulas, I., Kostenidou, E., Zampas, P., Theodosi, C., Kouvarakis, G.,
682 Canonaco, F., Prévôt, A. S. H., Nenes, A., Pandis, S. N., and Mihalopoulos, N.:
683 Processing of biomass-burning aerosol in the eastern Mediterranean during summertime,
684 *Atmos. Chem. Phys.*, 14, 4793-4807, doi:10.5194/acp-14-4793-2014, 2014.

685 Canagaratna, M., Jayne, J., Jimenez, J. L., Allan, J. A., Alfarra, R., Zhang, Q., Onasch, T.,
686 Drewnick, F., Coe, H., Middlebrook, A., Delia, A., Williams, L., Trimborn, A., Northway,
687 M., Kolb, C., Davidovits, P., and Worsnop, D.: Chemical and microphysical
688 characterization of aerosols via Aerosol Mass Spectrometry, *Mass Spectrom. Rev.*, 26,
689 185-222, 2007.

690 Canonaco, F., Crippa, M., Slowik, J. G., Baltensperger, U., and Prévôt, A. S. H.: SoFi, an
691 IGOR-based interface for the efficient use of the generalized multilinear engine (ME-2)
692 for the source apportionment: ME-2 application to aerosol mass spectrometer data,
693 *Atmos. Meas. Tech.*, 6, 3649-3661, doi:10.5194/amt-6-3649-2013, 2013.

694 Cheng, Y., Engling, G., He, K.-B., Duan, F.-K., Ma, Y.-L., Du, Z.-Y., Liu, J.-M., Zheng, M.,
695 and Weber, R. J.: Biomass burning contribution to Beijing aerosol, *Atmos. Chem. Phys.*,
696 13, 7765-7781, doi:10.5194/acp-13-7765-2013, 2013.

697 Crippa, M., DeCarlo, P. F., Slowik, J. G., Mohr, C., Heringa, M. F., Chirico, R., Poulain, L.,
698 Freutel, F., Sciare, J., Cozic, J., Di Marco, C. F., Elsasser, M., Nicolas, J. B.,
699 Marchand, N., Abidi, E., Wiedensohler, A., Drewnick, F., Schneider, J., Borrmann, S.,
700 Nemitz, E., Zimmermann, R., Jaffrezo, J.-L., Prévôt, A. S. H., and Baltensperger, U.:
701 Wintertime aerosol chemical composition and source apportionment of the organic
702 fraction in the metropolitan area of Paris, *Atmos. Chem. Phys.*, 13, 961-981,
703 doi:10.5194/acp-13-961-2013, 2013.

704 Crippa, M., Canonaco, F., Lanz, V. A., Äijälä M., Allan, J. D., Carbone, S., Capes, G.,
705 Ceburnis, D., Dall'Osto, M., Day, D. A., DeCarlo, P. F., Ehn, M., Eriksson, A., Freney, E.,
706 Hildebrandt Ruiz, L., Hillamo, R., Jimenez, J. L., Junninen, H., Kiendler-Scharr, A.,
707 Kortelainen, A.-M., Kulmala, M., Laaksonen, A., Mensah, A. A., Mohr, C., Nemitz, E.,
708 O'Dowd, C., Ovadnevaite, J., Pandis, S. N., Petäjä T., Poulain, L., Saarikoski, S.,
709 Sellegri, K., Swietlicki, E., Tiitta, P., Worsnop, D. R., Baltensperger, U., and Prévôt, A. S.
710 H.: Organic aerosol components derived from 25 AMS data sets across Europe using a
711 consistent ME-2 based source apportionment approach, *Atmos. Chem. Phys.*, 14,
712 6159-6176, doi:10.5194/acp-14-6159-2014, 2014.

713 Cubison, M. J., Ortega, A. M., Hayes, P. L., Farmer, D. K., Day, D., Lechner, M. J.,
714 Brune, W. H., Apel, E., Diskin, G. S., Fisher, J. A., Fuelberg, H. E., Hecobian, A.,
715 Knapp, D. J., Mikoviny, T., Riemer, D., Sachse, G. W., Sessions, W., Weber, R. J.,
716 Weinheimer, A. J., Wisthaler, A., and Jimenez, J. L.: Effects of aging on organic aerosol
717 from open biomass burning smoke in aircraft and laboratory studies, *Atmos. Chem.*
718 *Phys.*, 11, 12049-12064, doi:10.5194/acp-11-12049-2011, 2011.

719 DeCarlo, P. F., Dunlea, E. J., Kimmel, J. R., Aiken, A. C., Sueper, D., Crouse, J.,
720 Wennberg, P. O., Emmons, L., Shinozuka, Y., Clarke, A., Zhou, J., Tomlinson, J.,
721 Collins, D. R., Knapp, D., Weinheimer, A. J., Montzka, D. D., Campos, T., and
722 Jimenez, J. L.: Fast airborne aerosol size and chemistry measurements above Mexico
723 City and Central Mexico during the MILAGRO campaign, *Atmos. Chem. Phys.*, 8,
724 4027-4048, doi:10.5194/acp-8-4027-2008, 2008.

725 DeCarlo, P. F., Ulbrich, I. M., Crouse, J., de Foy, B., Dunlea, E. J., Aiken, A. C., Knapp, D.,
726 Weinheimer, A. J., Campos, T., Wennberg, P. O., and Jimenez, J. L.: Investigation of the
727 sources and processing of organic aerosol over the Central Mexican Plateau from
728 aircraft measurements during MILAGRO, *Atmos. Chem. Phys.*, 10, 5257-5280,
729 doi:10.5194/acp-10-5257-2010, 2010.

730 de Gouw, J. A., Middlebrook, A. M., Warneke, C., Goldan, P. D., Kuster, W. C., Roberts, J.
731 M., Fehsenfeld, F. C., Worsnop, D. R., Canagaratna, M. R., Pszenny, A. A. P., Keene, W.
732 C., Marchewka, M., Bertman, S. B., and Bates, T. S.: Budget of organic carbon in a
733 polluted atmosphere: Results from the New England Air Quality Study in 2002, *J.*
734 *Geophys. Res. Atmos.*, 110, D16305, 2005.

735 Ding, A. J., Fu, C. B., Yang, X. Q., Sun, J. N., Petäjä T., Kerminen, V.-M., Wang, T., Xie, Y.,
736 Herrmann, E., Zheng, L. F., Nie, W., Liu, Q., Wei, X. L., and Kulmala, M.: Intense
737 atmospheric pollution modifies weather: a case of mixed biomass burning with fossil
738 fuel combustion pollution in eastern China, *Atmos. Chem. Phys.*, 13, 10545-10554,
739 doi:10.5194/acp-13-10545-2013, 2013.

740 Draxler, R. R., Rolph, G. D.: HYSPLIT (HYbrid Single-Particle Lagrangian Integrated
741 Trajectory) Model Access via NOAA ARL READY Website. NOAA Air Resources
742 Laboratory, Silver Spring, MD. <http://www.arl.noaa.gov/ready/hysplit4.html>, 2003.

743 Du, H. H., Kong, L.D., Cheng, T.T., Chen, J.M., Du, J.F., Li, L., Xia, X.G., Leng, C.P., Huang,
744 G. H.: Insights into summertime haze pollution events over Shanghai based on online
745 water-soluble ionic composition of aerosols, *Atmos. Environ.*, 45, 5131-5137, 2011.

746 Dunlea, E. J., DeCarlo, P. F., Aiken, A. C., Kimmel, J. R., Peltier, R. E., Weber, R. J.,
747 Tomlinson, J., Collins, D. R., Shinozuka, Y., McNaughton, C. S., Howell, S. G., Clarke,
748 A. D., Emmons, L. K., Apel, E. C., Pfister, G. G., van Donkelaar, A., Martin, R. V.,
749 Millet, D. B., Heald, C. L., and Jimenez, J. L.: Evolution of Asian aerosols during
750 transpacific transport in INTEX-B, *Atmos. Chem. Phys.*, 9, 7257-7287,
751 doi:10.5194/acp-9-7257-2009, 2009.

752 Ge, W. Z., Chen, R. J., Song, W. M., and Kan, H. D.: Daily visibility and hospital admission
753 in Shanghai, China, *Biomed Environ. Sci.*, 24(2): 117-121, 2011.

754 Gilardoni, S., Liu, S., Takahama, S., Russell, L. M., Allan, J. D., Steinbrecher, R., Jimenez, J.
755 L., De Carlo, P. F., Dunlea, E. J., and Baumgardner, D.: Characterization of organic
756 ambient aerosol during MIRAGE 2006 on three platforms, *Atmos. Chem. Phys.*, 9,
757 5417-5432, doi:10.5194/acp-9-5417-2009, 2009.

758 Grieshop, A. P., Donahue, N. M., and Robinson, A. L.: Laboratory investigation of
759 photochemical oxidation of organic aerosol from wood fires 2: analysis of aerosol mass
760 spectrometer data, *Atmos. Chem. Phys.*, 9, 2227-2240, doi:10.5194/acp-9-2227-2009,
761 2009.

762 He, L.-Y., Lin, Y., Huang, X.-F., Guo, S., Xue, L., Su, Q., Hu, M., Luan, S.-J., and
763 Zhang, Y.-H.: Characterization of high-resolution aerosol mass spectra of primary
764 organic aerosol emissions from Chinese cooking and biomass burning, *Atmos. Chem.*
765 *Phys.*, 10, 11535-11543, doi:10.5194/acp-10-11535-2010, 2010.

766 Healy, R. M., Sciare, J., Poulain, L., Crippa, M., Wiedensohler, A., Prévôt, A. S. H.,
767 Baltensperger, U., Sarda-Estève, R., McGuire, M. L., Jeong, C.-H., McGillicuddy, E.,

768 O'Connor, I. P., Sodeau, J. R., Evans, G. J., and Wenger, J. C.: Quantitative
769 determination of carbonaceous particle mixing state in Paris using single-particle mass
770 spectrometer and aerosol mass spectrometer measurements, *Atmos. Chem. Phys.*, 13,
771 9479-9496, doi:10.5194/acp-13-9479-2013, 2013.

772 Heringa, M. F., DeCarlo, P. F., Chirico, R., Tritscher, T., Dommen, J., Weingartner, E., Richter,
773 R., Wehrle, G., Prévôt, A. S. H., and Baltensperger, U.: Investigations of primary and
774 secondary particulate matter of different wood combustion appliances with a
775 high-resolution time-of-flight aerosol mass spectrometer, *Atmos. Chem. Phys.*, 11,
776 5945-5957, doi:10.5194/acp-11-5945-2011, 2011.

777 Hu, W. W., Hu, M., Yuan, B., Jimenez, J. L., Tang, Q., Peng, J. F., Hu, W., Shao, M.,
778 Wang, M., Zeng, L. M., Wu, Y. S., Gong, Z. H., Huang, X. F., and He, L. Y.: Insights on
779 organic aerosol aging and the influence of coal combustion at a regional receptor site of
780 central eastern China, *Atmos. Chem. Phys.*, 13, 10095-10112,
781 doi:10.5194/acp-13-10095-2013, 2013.

782 Huang, X.-F., He, L.-Y., Hu, M., Canagaratna, M. R., Sun, Y., Zhang, Q., Zhu, T., Xue, L.,
783 Zeng, L.-W., Liu, X.-G., Zhang, Y.-H., Jayne, J. T., Ng, N. L., and Worsnop, D. R.:
784 Highly time-resolved chemical characterization of atmospheric submicron particles
785 during 2008 Beijing Olympic Games using an Aerodyne High-Resolution Aerosol Mass
786 Spectrometer, *Atmos. Chem. Phys.*, 10, 8933-8945, doi:10.5194/acp-10-8933-2010,
787 2010.

788 Huang, X.-F., He, L.-Y., Hu, M., Canagaratna, M. R., Kroll, J. H., Ng, N. L., Zhang, Y.-H.,
789 Lin, Y., Xue, L., Sun, T.-L., Liu, X.-G., Shao, M., Jayne, J. T., and Worsnop, D. R.:
790 Characterization of submicron aerosols at a rural site in Pearl River Delta of China using
791 an Aerodyne High-Resolution Aerosol Mass Spectrometer, *Atmos. Chem. Phys.*, 11,
792 1865-1877, doi:10.5194/acp-11-1865-2011, 2011.

793 Huang, X.-F., He, L.-Y., Xue, L., Sun, T.-L., Zeng, L.-W., Gong, Z.-H., Hu, M., and Zhu, T.:
794 Highly time-resolved chemical characterization of atmospheric fine particles during
795 2010 Shanghai World Expo, *Atmos. Chem. Phys.*, 12, 4897-4907,
796 doi:10.5194/acp-12-4897-2012, 2012.

797 Huang, X.-F., Xue, L., Tian, D.-X., Shao, W.-W., Sun, T.-L., Gong, Z.-H., Ju, W.-W., Jiang,
798 B., Hu, M., and He, L.-Y.: Highly time-resolved carbonaceous aerosol characterization
799 in Yangtze River Delta of China: Composition, mixing state and secondary formation,
800 *Atmos. Environ.*, 64, 200-207, 2013.

801 Huffman, J. A., Docherty, K. S., Aiken, A. C., Cubison, M. J., Ulbrich, I. M., DeCarlo, P. F.,
802 Sueper, D., Jayne, J. T., Worsnop, D. R., Ziemann, P. J., and Jimenez, J. L.:
803 Chemically-resolved aerosol volatility measurements from two megacity field studies,
804 *Atmos. Chem. Phys.*, 9, 7161-7182, doi:10.5194/acp-9-7161-2009, 2009.

805 Jimenez, J. L., Canagaratna, M. R., Donahue, N. M., Prévôt, A. S. H., Zhang, Q., Kroll, J. H.,
806 DeCarlo, P. F., Allan, J. D., Coe, H., Ng, N. L., Aiken, A. C., Docherty, K. S., Ulbrich, I.
807 M., Grieshop, A. P., Robinson, A. L., Duplissy, J., Smith, J. D., Wilson, K. R., Lanz, V.
808 A., Hueglin, C., Sun, Y. L., Tian, J., Laaksonen, A., Raatikainen, T., Rautiainen, J.,
809 Vaattovaara, P., Ehn, M., Kulmala, M., Tomlinson, J. M., Collins, D. R., Cubison, M. J.,
810 E, Dunlea, J., Huffman, J. A., Onasch, T. B., Alfarra, M. R., Williams, P. I., Bower, K.,
811 Kondo, Y., Schneider, J., Drewnick, F., Borrmann, S., Weimer, S., Demerjian, K.,
812 Salcedo, D., Cottrell, L., Griffin, R., Takami, A., Miyoshi, T., Hatakeyama, S., Shimono,
813 A., Sun, J. Y., Zhang, Y. M., Dzepina, K., Kimmel, J. R., Sueper, D., Jayne, J. T.,
814 Herndon, S. C., Trimborn, A. M., Williams, L. R., Wood, E. C., Middlebrook, A. M.,
815 Kolb, C. E., Baltensperger, U., and Worsnop, D. R.: Evolution of organic aerosols in the
816 atmosphere, *Science*, 326, 1525-1529, 2009.

817 Justice, C. O., Giglio, L., Korontzi, S., Owens, J., Morisette, J.T., Roy, D., Descloitres, J.,
818 Alleaume, S., Petitcolin, F., Kaufman, Y.: The MODIS fire products, *Remote Sens.*
819 *Environ.*, 83, 244-262, 2002.

820 Kaufman, Y. J., Tanre, D., and Boucher, O.: A satellite view of aerosols in the climate system,
821 *Nature*, 419: 215-23, 2002.

822 Kaufman, Y. J., Ichoku, C., Giglio, L., Korontzi, S., Chu, D. A., Hao, W. M., Li R. R., Justice,
823 C. O.: Fire and smoke observed from the Earth Observing System MODIS
824 instrument-products, validation, and operational use, *Int. J. Remote Sensing*, 24,
825 1765-781, 2003.

826 Kawamura, K., Tachibana, E., Okuzawa, K., Aggarwal, S. G., Kanaya, Y., and Wang, Z. F.:
827 High abundances of water-soluble dicarboxylic acids, ketocarboxylic acids and
828 α -dicarbonyls in the mountaintop aerosols over the North China Plain during wheat
829 burning season, *Atmos. Chem. Phys.*, 13, 8285-8302, doi:10.5194/acp-13-8285-2013,
830 2013.

831 Lanz, V. A., Alfarra, M. R., Baltensperger, U., Buchmann, B., Hueglin, C., and
832 Prévôt, A. S. H.: Source apportionment of submicron organic aerosols at an urban site by
833 factor analytical modelling of aerosol mass spectra, *Atmos. Chem. Phys.*, 7, 1503-1522,
834 doi:10.5194/acp-7-1503-2007, 2007.

835 Latham, T. L., Beyersdorf, A. J., Thornhill, K. L., Winstead, E. L., Cubison, M. J., Hecobian,
836 A., Jimenez, J. L., Weber, R. J., Anderson, B. E., and Nenes, A.: Analysis of CCN
837 activity of Arctic aerosol and Canadian biomass burning during summer 2008, *Atmos.*
838 *Chem. Phys.*, 13, 2735-2756, doi:10.5194/acp-13-2735-2013, 2013.

839 Lee, T., Sullivan, A. P., Mack, L., Jimenez, J. L., Kreidenweis, S. M., Onasch, T. B., Worsnop,
840 D. R., Malm, W., Wold, C. E., Hao, W. M., and Collett, J. L.: Chemical smoke marker

841 emissions during flaming and smoldering phases of laboratory open burning of wildland
842 fuels, *Aerosol Sci. Tech.*, 44, 1-5, 2010.

843 Li, X. H., Wang, S. X., Duan, L., Hao, J. M., Li, Y. S., and Yang, L.: Particulate and trace gas
844 emissions from open burning of wheat straw and corn stover in China, *Environ. Sci.*
845 *Technol.*, 41 (17): 6052-6058, 2007.

846 Lipsky, E. M. and Robinson, A. L.: Effects of dilution on fine particle mass and partitioning
847 of semivolatile organics in diesel exhaust and wood smoke, *Environ. Sci. Technol.*, 40,
848 155–162, 2006.

849 Liu, D., Allan, J., Corris, B., Flynn, M., Andrews, E., Ogren, J., Beswick, K., Bower, K.,
850 Burgess, R., Choularton, T., Dorsey, J., Morgan, W., Williams, P. I., and Coe, H.:
851 Carbonaceous aerosols contributed by traffic and solid fuel burning at a polluted rural
852 site in Northwestern England, *Atmos. Chem. Phys.*, 11, 1603-1619,
853 doi:10.5194/acp-11-1603-2011, 2011.

854 Liu, D., Allan, J. D., Young, D. E., Coe, H., Beddows, D., Fleming, Z. L., Flynn, M. J.,
855 Gallagher, M. W., Harrison, R. M., Lee, J., Prevot, A. S. H., Taylor, J. W., Yin, J.,
856 Williams, P. I., and Zotter, P.: Size distribution, mixing state and source apportionments
857 of black carbon aerosols in London during winter time, *Atmos. Chem. Phys. Discuss.*,
858 14, 16291-16349, doi:10.5194/acpd-14-16291-2014, 2014.

859 Maenhaut, W., Vermeylen, R., Claeys, M., Vercauteren, J., Matheussen, C., Roekens, E.:
860 Assessment of the contribution from wood burning to the PM₁₀ aerosol in Flanders,
861 Belgium, *Sci. Total Environ.*, 437, 226-236, 2012.

862 Middlebrook, A. M., Bahreini, R., Jimenez, J. L., and Canagaratna, M. R.: Evaluation of
863 composition-dependent collection efficiencies for the aerodyne aerosol mass
864 spectrometer using field data, *Aerosol Sci. Tech.*, 46, 258-271, 2011.

865 Mohr, C., Huffman, J. A., Cubison, M. J., Aiken, A. C., Docherty, K. S., Kimmel, J. R.,
866 Ulbrich, I. M., Hannigan, M., and Jimenez, J. L.: Characterization of primary organic
867 aerosol emissions from meat cooking, trash burning, and motor vehicles with
868 High-Resolution Aerosol Mass Spectrometry and comparison with ambient and chamber
869 observations, *Environ. Sci. Technol.*, 43, 2443-2449, 2009.

870 Mohr, C., DeCarlo, P. F., Heringa, M. F., Chirico, R., Slowik, J. G., Richter, R., Reche, C.,
871 Alastuey, A., Querol, X., Seco, R., Peñuelas, J., Jiménez, J. L., Crippa, M.,
872 Zimmermann, R., Baltensperger, U., and Prévôt, A. S. H.: Identification and
873 quantification of organic aerosol from cooking and other sources in Barcelona using
874 aerosol mass spectrometer data, *Atmos. Chem. Phys.*, 12, 1649-1665,
875 doi:10.5194/acp-12-1649-2012, 2012.

876 Ng, N. L., Canagaratna, M. R., Zhang, Q., Jimenez, J. L., Tian, J., Ulbrich, I. M., Kroll, J. H.,
877 Docherty, K. S., Chhabra, P. S., Bahreini, R., Murphy, S. M., Seinfeld, J. H.,
878 Hildebrandt, L., Donahue, N. M., DeCarlo, P. F., Lanz, V. A., Prévôt, A. S. H., Dinar, E.,
879 Rudich, Y., and Worsnop, D. R.: Organic aerosol components observed in Northern
880 Hemispheric datasets from aerosol mass spectrometry, *Atmos. Chem. Phys.*, 10,
881 4625-4641, doi:10.5194/acp-10-4625-2010, 2010.

882 Ng, N. L., Herndon, S. C., Trimborn, A., Canagaratna, M. R., Croteau, P. L., Onasch, T. B.,
883 Sueper, D., Worsnop, D. R., Zhang, Q., Sun, Y. L., and Jayne, J. T.: An aerosol chemical
884 speciation monitor (ACSM) for routine monitoring of the composition and mass
885 concentrations of ambient aerosol, *Aerosol Sci. Technol.*, 45: 7, 770 -784, 2011a.

886 Ng, N. L., Canagaratna, M. R., Jimenez, J. L., Chhabra, P. S., Seinfeld, J. H., and
887 Worsnop, D. R.: Changes in organic aerosol composition with aging inferred from
888 aerosol mass spectra, *Atmos. Chem. Phys.*, 11, 6465-6474,
889 doi:10.5194/acp-11-6465-2011, 2011b.

890 Ng, N. L., Canagaratna, M. R., Jimenez, J. L., Zhang, Q., Ulbrich, I. M., and Worsnop, D. R.:
891 Real-time methods for estimating organic component mass concentrations from aerosol
892 mass spectrometer data, *Environ. Sci. Technol.*, 45, 910-916, 2011c.

893 Paatero, P.: Least squares formulation of robust non-negative factor analysis, *Chemom. Intell.*
894 *Lab. Syst.*, 37, 23-35, 1997.

895 Paatero, P.: The multilinear engine – A table-driven, least squares program for solving
896 multilinear problems, including the n-way parallel factor analysis model, *J. Comput.*
897 *Graph. Stat.*, 8, 854–888, 1999.

898 Ramanathan, V., Crutzen, P. J, Kiehl, J. T., and Rosenfeld, D.: Atmosphere, aerosols, climate,
899 and the hydrological cycle, *Science*, 294, 2119–2124, 2001.

900 Reche, C., Viana, M., Amato, F., Alastuey, A., Moreno, T., Hillamo, R., Teinila, K., Saarnio,
901 K., Seco, R., Penuelas, J., Mohr, C., Prévôt, A. S. H., and Querol, X.: Biomass burning
902 contributions to urban aerosols in a coastal Mediterranean City, *Sci. Total Environ.*, 427,
903 175-190, 2012.

904 Robinson, A. L., Donahue, N. M., Shrivastava, M. K., Weitkamp, E. A., Sage, A. M.,
905 Grieshop, A. P., Lane, T. E., Pierce, J. R., and Pandis, S. N.: Rethinking organic aerosols:
906 Semivolatile emissions and photochemical aging, *Science*, 315, 1259–1262,
907 doi:10.1126/science.1133061, 2007.

908 Sandradewi, J., Prevot, A. S. H., Szidat, S., Perron, N., Alfarra, M. R., Lanz, V. A.,
909 Weingartner, E., and Baltensperger, U.: Using aerosol light absorption measurements for
910 the quantitative determination of wood burning and traffic emission contributions to
911 particulate matter, *Environ. Sci. Technol.*, 42, 3316–3323, 2008.

912 Sun, J. Y., Zhang, Q., Canagaratna, M. R., Zhang, Y. M., Ng, N. L., Sun, Y. L., Jayne, J. T.,
913 Zhang, X. C., Zhang, X. Y., and Worsnop, D. R.: Highly time- and size-resolved

914 characterization of submicron aerosol particles in Beijing using an Aerodyne Aerosol
915 Mass Spectrometer, *Atmos. Environ.*, 44, 131-140, 2010.

916 Sun, Y.-L., Zhang, Q., Schwab, J. J., Demerjian, K. L., Chen, W.-N., Bae, M.-S., Hung, H.-M.,
917 Hogrefe, O., Frank, B., Rattigan, O. V., and Lin, Y.-C.: Characterization of the sources
918 and processes of organic and inorganic aerosols in New York city with a high-resolution
919 time-of-flight aerosol mass spectrometer, *Atmos. Chem. Phys.*, 11, 1581-1602,
920 doi:10.5194/acp-11-1581-2011, 2011a.

921 Sun, Y. L., Zhang, Q., Schwab, J. J., Chen, W. N., Bae, M. S., Lin, Y. C., Hung, H. M., and
922 Demerjian, K. L.: A case study of aerosol processing and evolution in summer in New
923 York City, *Atmos. Chem. Phys.*, 11, 12737-12750, doi:10.5194/acp-11-12737-2011,
924 2011b.

925 Sun, Y. L., Wang, Z. F., Dong, H. B., Yang, T., Li, J., Pan, X. L., Chen, P., and Jayne, J. T.:
926 Characterization of summer organic and inorganic aerosols in Beijing, China with an
927 Aerosol Chemical Speciation Monitor, *Atmos. Environ.*, 51, 250-259, 2012.

928 Sun, Y. L., Wang, Z. F., Fu, P. Q., Yang, T., Jiang, Q., Dong, H. B., Li, J., and Jia, J. J.:
929 Aerosol composition, sources and processes during wintertime in Beijing, China, *Atmos.*
930 *Chem. Phys.*, 13, 4577-4592, doi:10.5194/acp-13-4577-2013, 2013.

931 Takegawa, N., Miyakawa, T., Kondo, Y., Jimenez, J. L., Zhang, Q., Worsnop, D. R., and
932 Fukuda, M.: Seasonal and diurnal variations of submicron organic aerosol in Tokyo
933 observed using the Aerodyne aerosol mass spectrometer, *J. Geophys. Res.*, 111, D11206,
934 2006.

935 Ulbrich, I. M., Canagaratna, M. R., Zhang, Q., Worsnop, D. R., and Jimenez, J. L.:
936 Interpretation of organic components from Positive Matrix Factorization of aerosol mass
937 spectrometric data, *Atmos. Chem. Phys.*, 9, 2891–2918, doi:10.5194/acp-9-2891-2009,
938 2009.

939 Wang, G. H., Kawamura, K., Xie, M. J., Hu, S. Y., Cao, J. J., An, Z. H., Weston J. G., and
940 Chow, J. C.: Organic molecular compositions and size distributions of Chinese summer
941 and autumn aerosols from Nanjing: characteristic haze event caused by wheat straw
942 burning, *Environ. Sci. Technol.*, 43 (17): 6493-6499, 2009a.

943 Wang, Y. Q., Zhang, X. Y., and Draxler, R. R.: TrajStat: GIS-based software that uses various
944 trajectory statistical analysis methods to identify potential sources from long-term air
945 pollution measurement data, *Environ. Modell. Softw.*, 24: 938-939, 2009b.

946 Watson, J. G.: Visibility: Science and regulation, *J. Air Waste Manage. Assoc.*, 52, 628-713,
947 2002.

948 Yee, L. D., Kautzman, K. E., Loza, C. L., Schilling, K. A., Coggon, M. M., Chhabra, P. S.,
949 Chan, M. N., Chan, A. W. H., Hersey, S. P., Crouse, J. D., Wennberg, P. O., Flagan, R.
950 C., and Seinfeld, J. H.: Secondary organic aerosol formation from biomass burning
951 intermediates: phenol and methoxyphenols, *Atmos. Chem. Phys.*, 13, 8019-8043,
952 doi:10.5194/acp-13-8019-2013, 2013.

953 Zhang, H., Ye, X., Cheng, T., Chen, J., Yang, X., Wang, L., Zhang, R.: A laboratory study of
954 agricultural crop residue combustion in China: Emission factors and emission inventory,
955 *Atmos. Environ.*, 42, 8432-8441, 2008.

956 Zhang, Q., Worsnop, D. R., Canagaratna, M. R., and Jimenez, J. L.: Hydrocarbon-like and
957 oxygenated organic aerosols in Pittsburgh: insights into sources and processes of organic
958 aerosols, *Atmos. Chem. Phys.*, 5, 3289-3311, doi:10.5194/acp-5-3289-2005, 2005a.

959 Zhang, Q., Alfarra, M.R. Worsnop, D., Allan, J. D., Coe, H., Cangaratna, M. R., Jimenez, J.
960 L.: Deconvolution and quantification of hydrocarbon-like and oxygenated organic
961 aerosols based on aerosol mass spectrometry, *Environ. Sci. Technol.*, 39, 4938-4952,
962 2005b.

963 Zhang, Q., Jimenez, J. L., Canagaratna, M. R., Allan, J. D, Coe, H., Ulbrich, I. M., Alfarra, M.

964 R., Takami, A., Middlebrook, A. M., Sun, Y. L., Dzepina, K., Dunlea, E., Docherty, K.,
965 DeCarlo, P. F., Salcedo, D., Onasch, T., Jayne, J. T., Miyoshi, T., Shimojo, A.,
966 Hatakeyama, S., Takegawa, N., Kondo, Y., Schneider, J., Drewnick, F., Borrmann, S.,
967 Weimer, S., Demerjian, K., Williams, P., Bower, K., Bahreini, R., Cottrell, L., Griffin, R.
968 J., Rautiainen, J., Sun, J. Y., Zhang, Y. M., Worsnop, D. R.: Ubiquity and dominance of
969 oxygenated species in organic aerosols in anthropogenically-influenced Northern
970 Hemisphere midlatitudes, *Geophys. Res. Lett.*, 34(13): L13801, 2007.

971 Zhang, Q., Jimenez, J. L., Canagaratna, M. R., Ulbrich, I. M., Ng, N. L., Worsnop, D. R., Sun,
972 Y. L.: Understanding atmospheric organic aerosols via factor analysis of aerosol mass
973 spectrometry: a review, *Anal. Bioanal. Chem.*, 401:3045-3067, 2011.

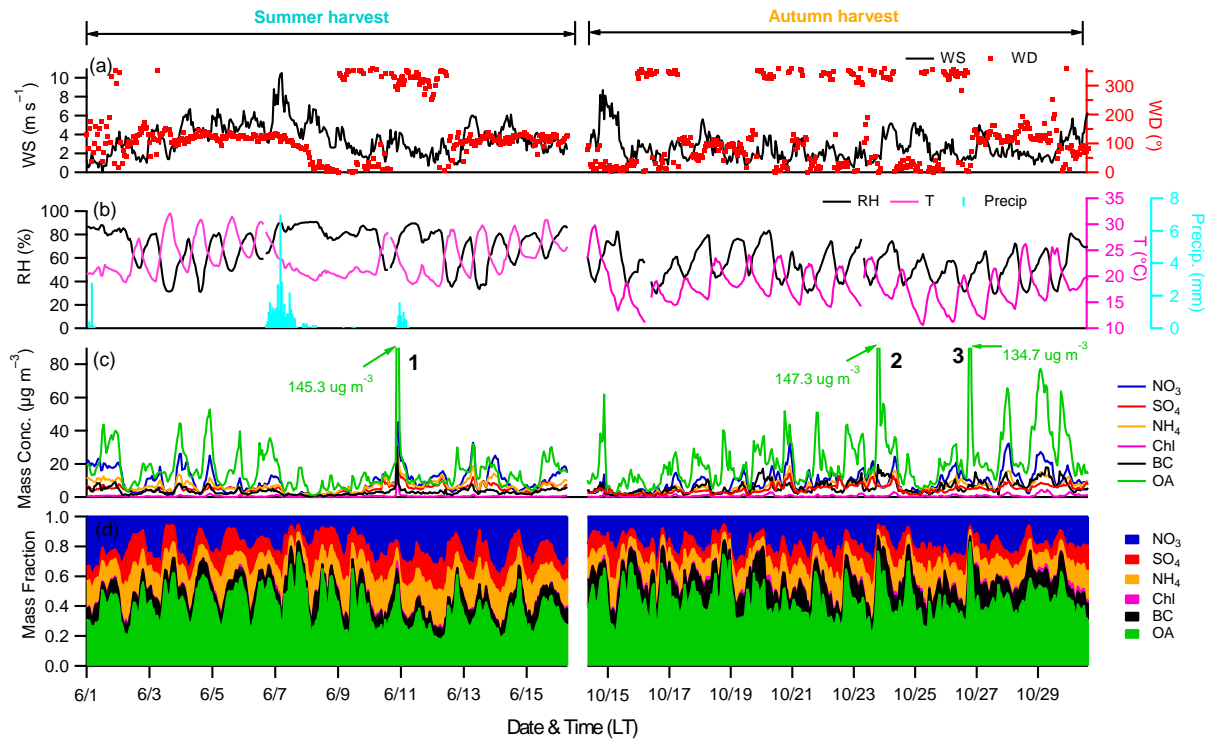
974

975 Table 1

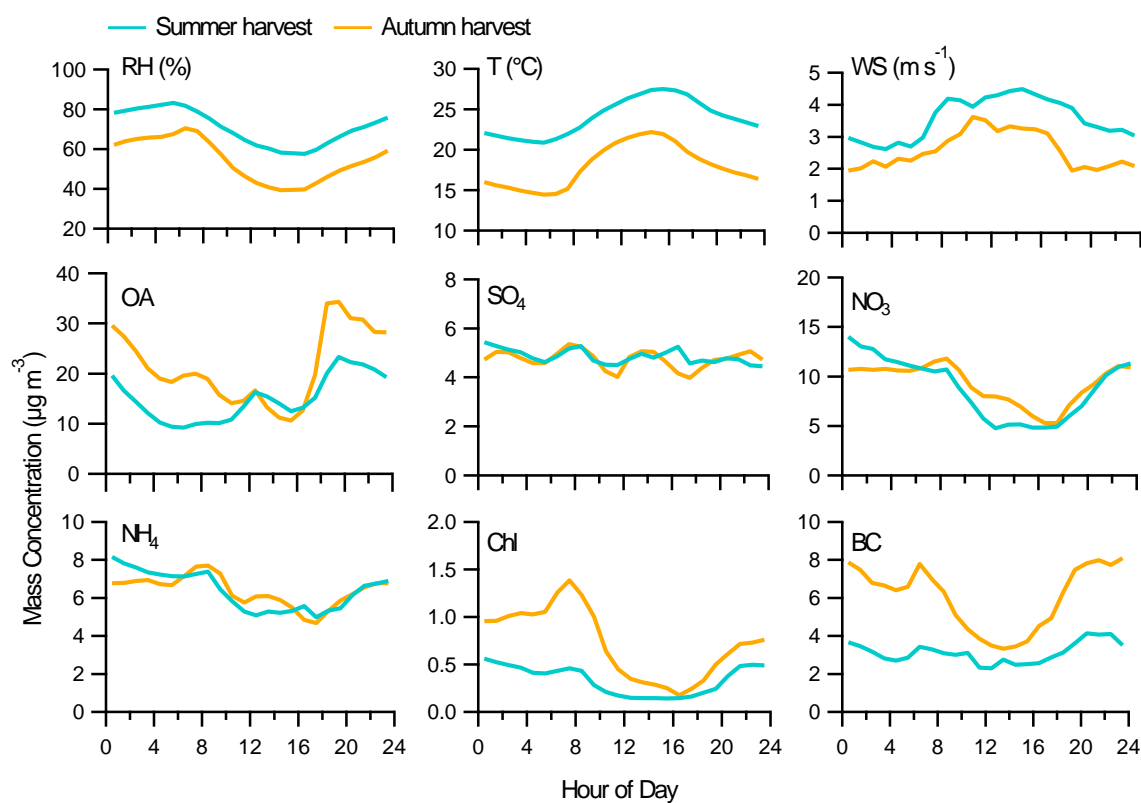
976 Mean mass concentrations ($\mu\text{g m}^{-3}$) and standard deviation (S.D.) of PM_{10} (NR- PM_{10} + BC) species, OA
977 components and meteorological factors (i.e. WS, RH, and T) during the harvest seasons.

	Summer harvest		Autumn harvest	
	Mean	S.D.	Mean	S.D.
Aerosol species				
NO_3	9.0	7.1	9.2	6.2
SO_4	5.0	2.4	4.7	2.5
NH_4	7.0	3.5	6.4	3.5
Chl	0.4	0.9	0.7	0.8
OA	15.4	12.8	22.3	17.5
BC	3.2	2.2	6.0	3.8
PM_{10}	38.5	24.3	46.4	27.0
OA components				
HOA + COA	2.2	2.4	5.7	7.6
BBOA	1.1	1.0	1.5	1.6
OOA-BB	4.1	4.6	6.5	7.3
OOA	7.1	3.6	6.6	3.2
Meteorological factors				
WS (m s^{-1})	3.5	1.7	2.6	1.4
RH (%)	70.7	15.3	54.3	13.7
T ($^{\circ}\text{C}$)	24.1	4.1	18.1	3.5

978



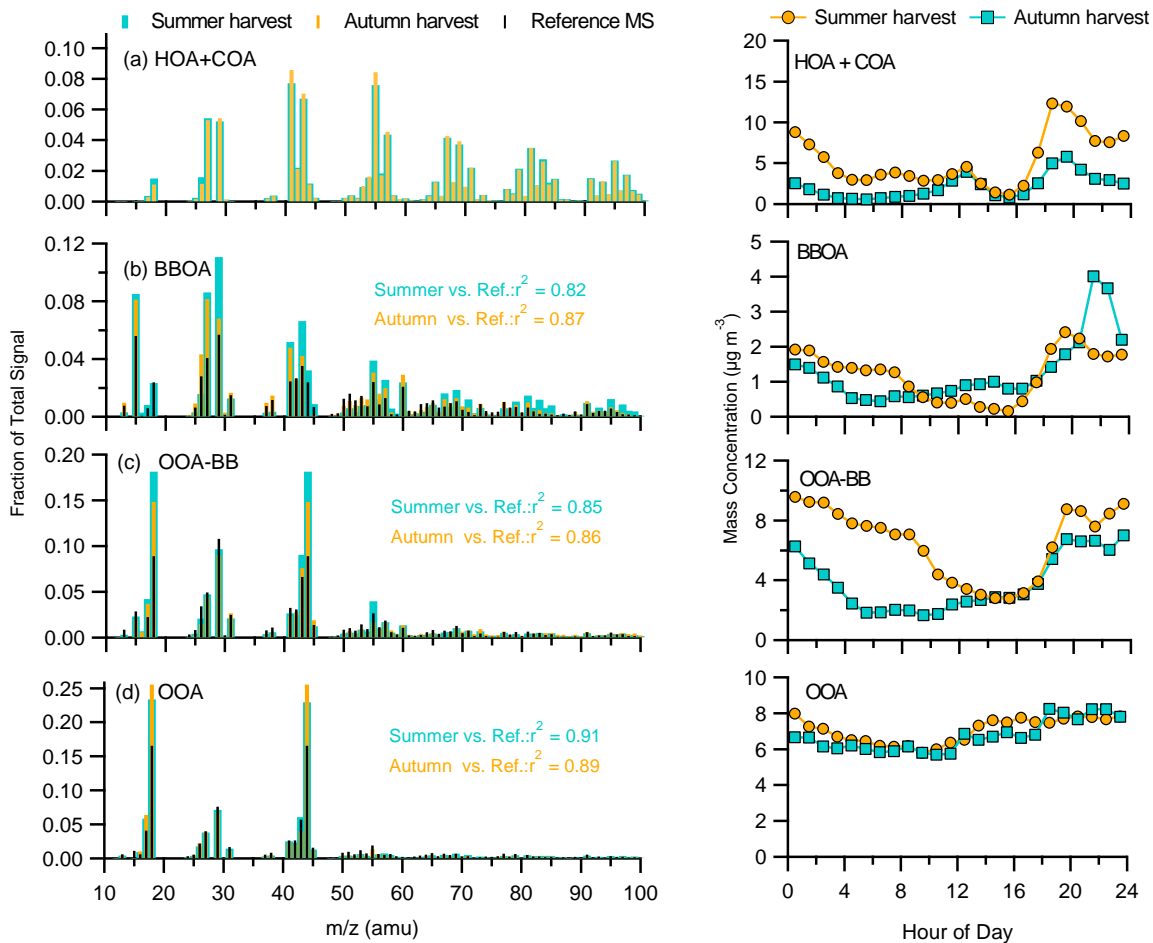
979
 980 **Fig. 1.** Time series of (a) wind speed (WS) and wind direction (WD); (b) relative humidity (RH),
 981 temperature (T) and precipitation (Precip); (c) submicron aerosol species, i.e., organic aerosol (OA),
 982 ammonium (NH_4), nitrate (NO_3), sulfate (SO_4), chloride (Chl) and black carbon (BC); and (d) mass
 983 fraction during the harvest seasons. Three case events are marked and discussed in the text.



985

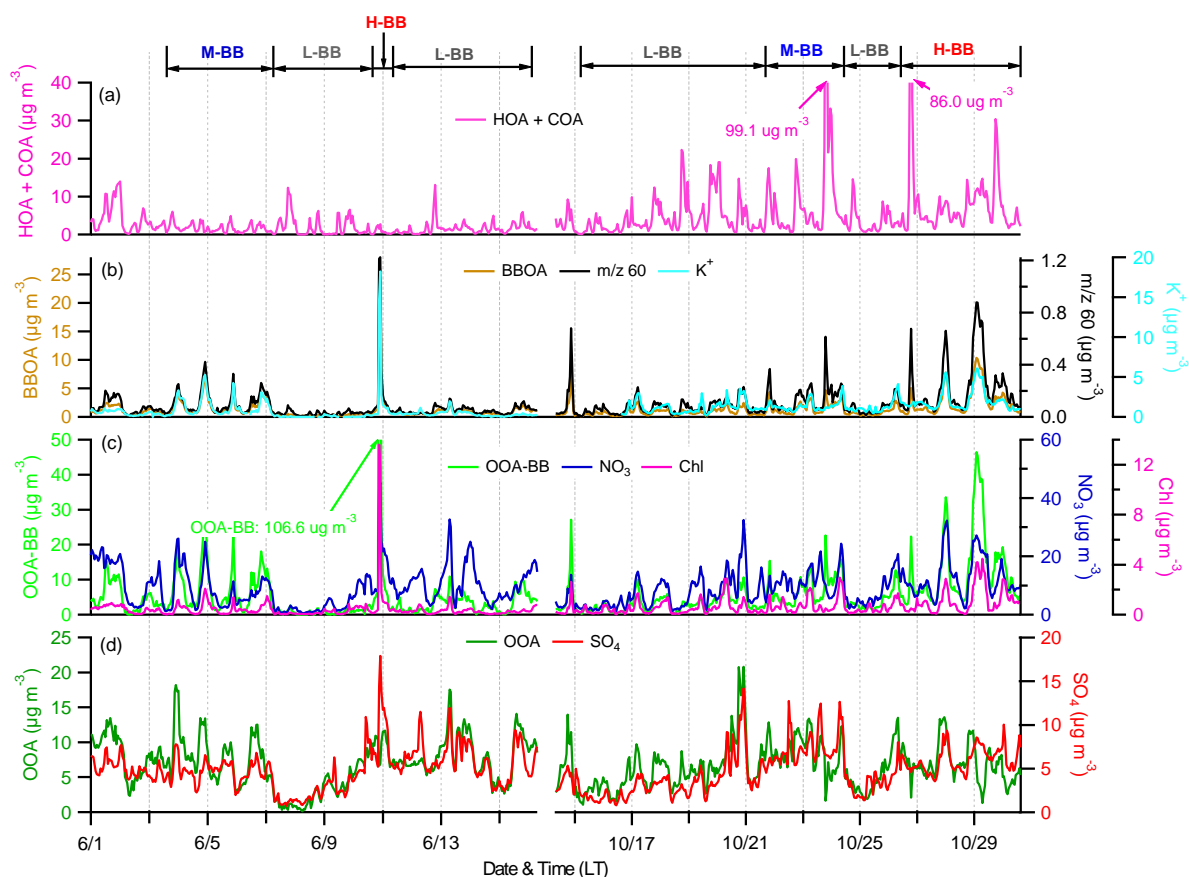
986 **Fig. 2.** Diurnal variation patterns of meteorological factors (i.e. RH, *T*, and WS), PM₁ species including
 987 organic aerosol (OA), nitrate (NO₃), sulfate (SO₄), ammonium (NH₄), chloride (Chl), and black carbon
 988 (BC) during the harvest seasons.

989



990
 991 **Fig. 3.** Mass spectra profiles (left) and diurnal variations (right) of four OA factors, i.e., hydrocarbon-like
 992 and cooking-emission related OA (HOA + COA), fresh biomass burning (BB) OA (BBOA), oxygenated
 993 BB-influenced OA (OOA-BB), and highly oxygenated OA (OOA). Note that: reference mass spectra (MS)
 994 are obtained from the results by Crippa et al. (2013), and oxygenated BBOA components have been
 995 resolved (OOA₂-BBOA).

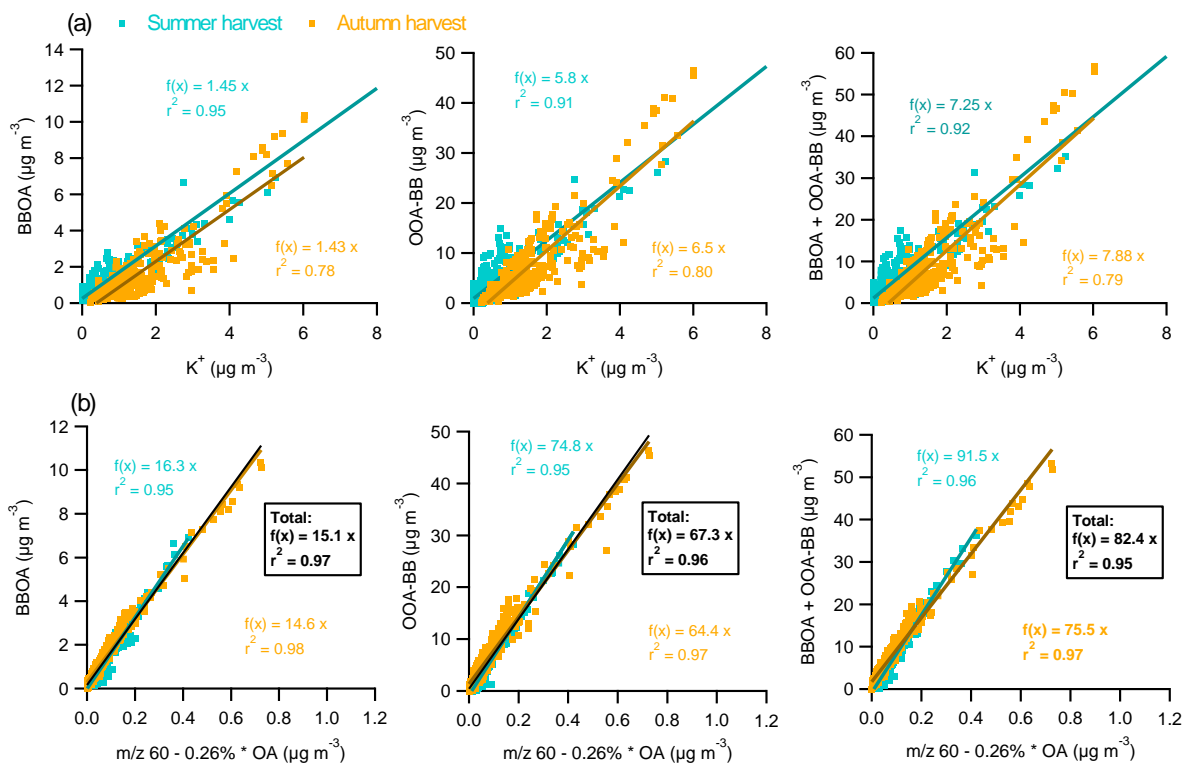
996



997

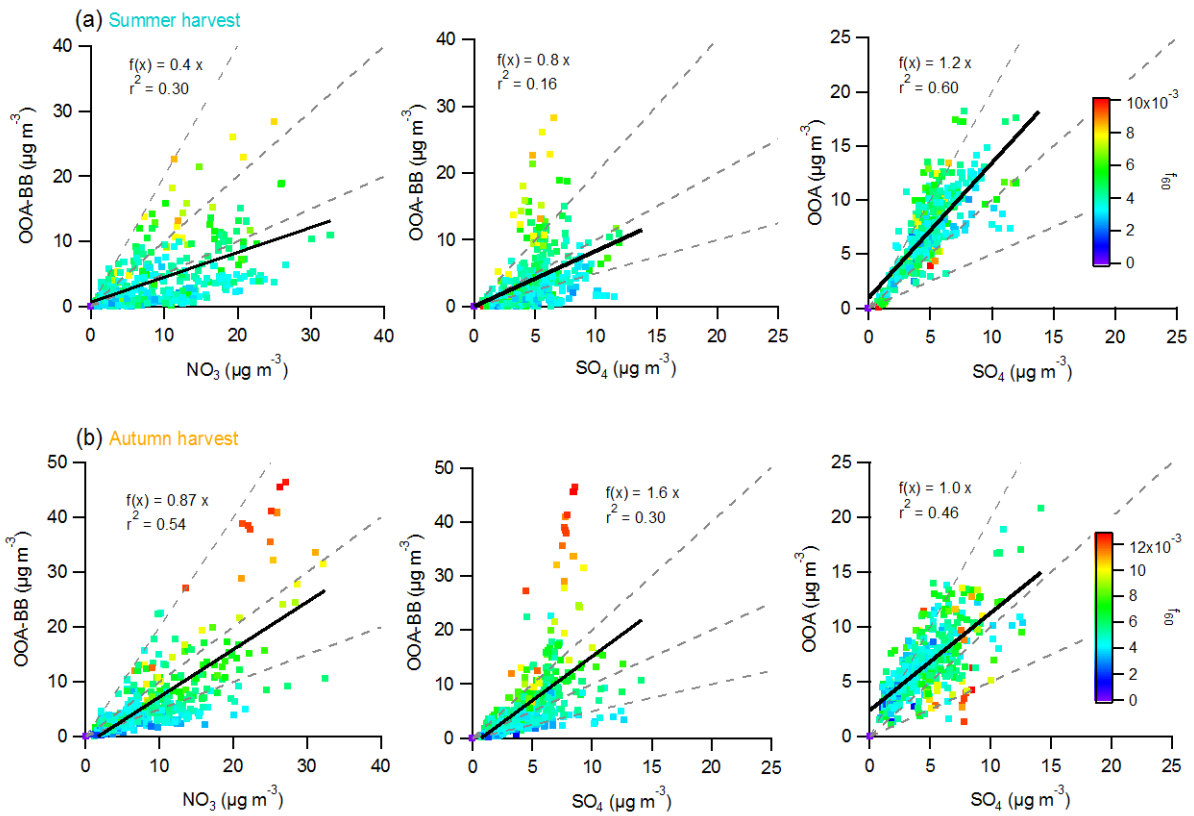
998 **Fig. 4.** Time series of OA factors (left) and relevant tracer species (right): **(a)** HOA + COA; **(b)** BBOA and
 999 a surrogate of levoglucosan (m/z 60) and potassium ion (K^+); **(c)** OOA-BB, nitrate and chloride; **(d)** OOA
 1000 and SO_4 . Note that different BBOA mass concentrations for low biomass burning period (L-BB), medium
 1001 biomass burning period (M-BB), and high biomass burning period (H-BB).

1002



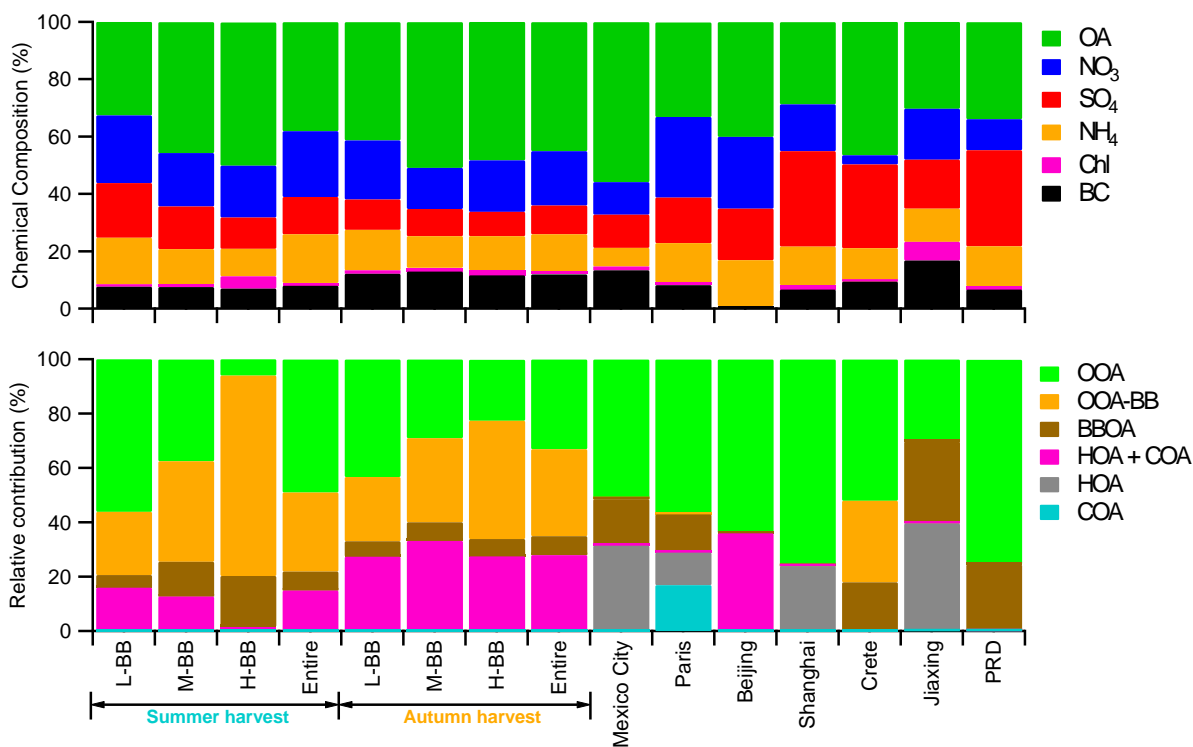
1003
 1004
 1005
 1006
 1007

Fig. 5. Comparison of biomass burning-related PMF factors (BBOA and OOA-BB) and biomass related species: (a) K^+ ; and (b) the ACSM m/z 60 minus $0.26\% \times \text{OA}$ (applied metric of background $f_{60} = 0.26\%$ of OA is discussed in the section 3.4 of the text) during the summer and autumn harvest.



1008
 1009
 1010
 1011
 1012

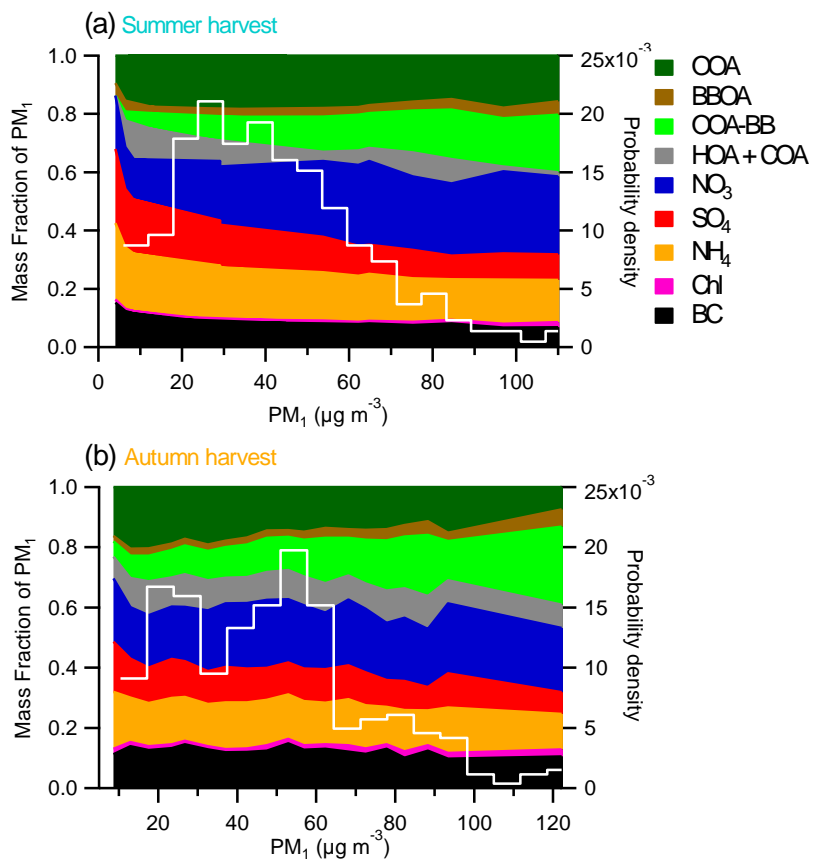
Fig. 6. Comparison of two kinds of oxygenated OA (OOA-BB and OOA) and two kinds of secondary inorganic species, i.e., nitrate (NO_3) and sulfate (SO_4), during the harvest seasons. Colored by the f_{60} as a biomass-burning marker. The three dashed lines in the plot refer to 2 : 1, 1 : 1, and 1 : 2 lines, respectively.



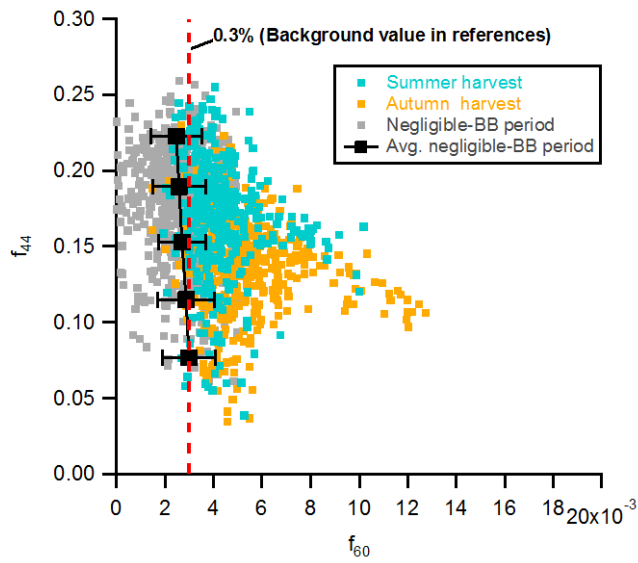
1013

1014 **Fig. 7.** Average relative contributions of PM₁ species and OA components for low biomass burning period
 1015 (L-BB), medium biomass burning period (M-BB), and high biomass burning period (H-BB), as well as
 1016 entire period during the harvest seasons and other sites including mega-cities (Mexico city, Paris, Beijing
 1017 and Shanghai), suburban area (Jiaxing), remote background site (Crete), and PRD (Pearl River Delta,
 1018 China). Note that OOA in this plot includes OOA₂-BBOA in Paris.

1019



1020
 1021 **Fig. 8.** The mass fractions of PM₁ species and OA components as a function of PM₁ mass loadings (left),
 1022 and probability density of PM₁ mass loadings (right, with the white lines in the plots) during the summer
 1023 and autumn harvest respectively.
 1024

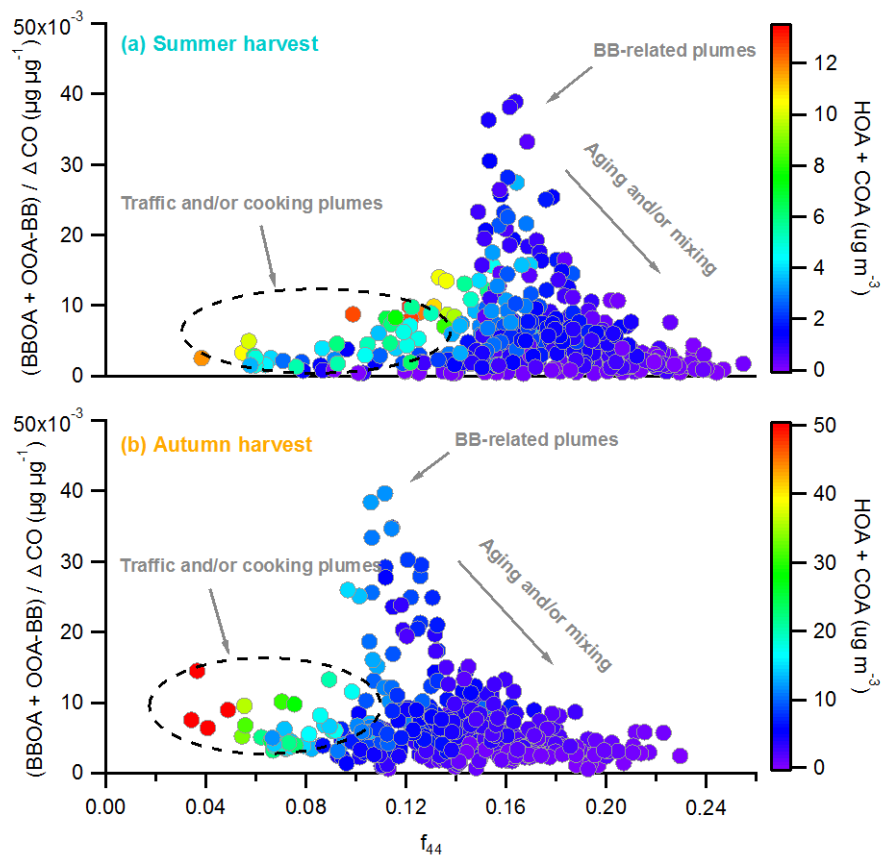


1025

1026 **Fig. 9.** Summary plots showing f_{44} vs. f_{60} for measurements with little or negligible biomass burning
 1027 influence. Colored by the summer harvest (blue), autumn harvest (orange), and little or negligible biomass
 1028 burning influence period (gray, July 1 to 8, 2013), respectively. Also shown is the average background
 1029 level of f_{60} (~0.3%, red dashed line) in other studies from Aiken et al. (2009) and Cubison et al. (2011) for
 1030 references.

1031

1032

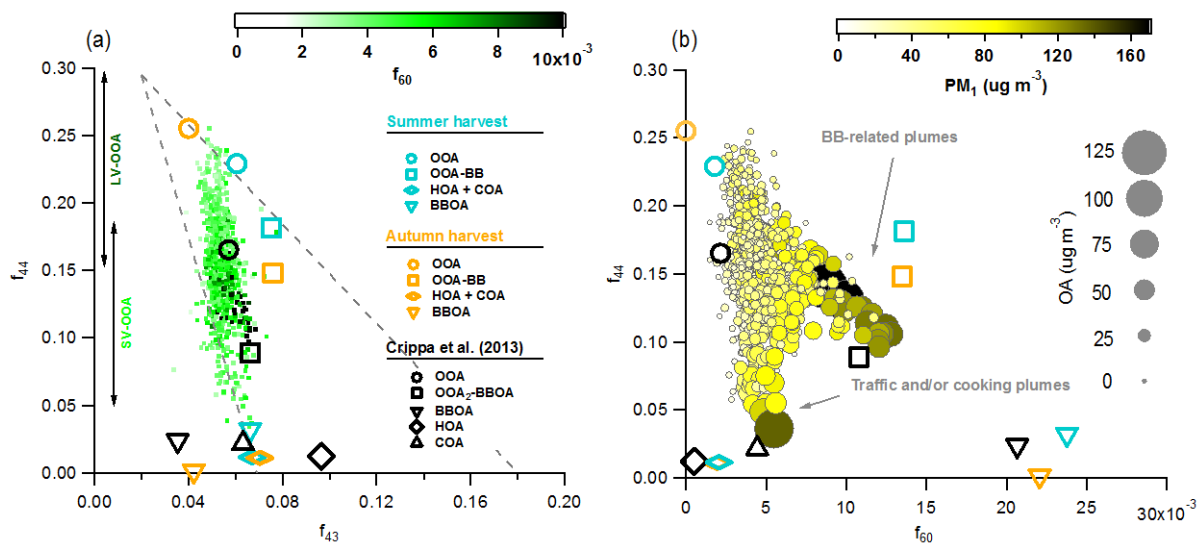


1033

1034 **Fig. 10.** The $(\text{BBOA} + \text{OOA-BB}) / \Delta\text{CO}$ ratio as a function of f_{44} during the summer and autumn harvest.

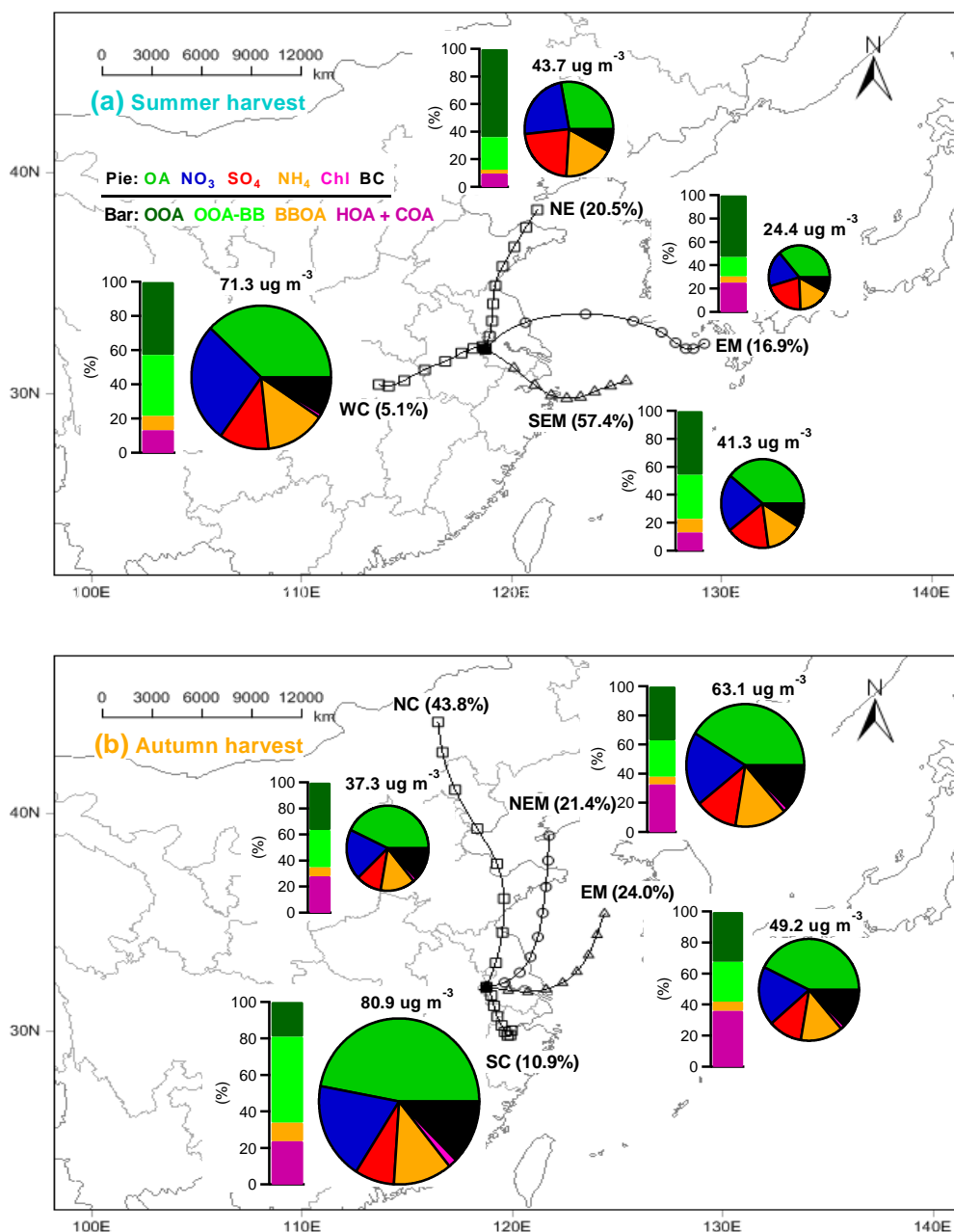
1035 Colored by the HOA + COA mass concentrations for the summer and autumn harvest.

1036



1037
 1038
 1039
 1040
 1041

Fig. 11. Summary plots showing (a) triangle plot (f_{44} vs. f_{43}), SV-OOA and LV-OOA indicate semi-volatile OOA and low-volatility OOA respectively. The dots are colored by f_{60} as a biomass-burning marker; (b) f_{44} as a function of f_{60} (f_{44} vs. f_{60}), colored by the PM_{10} mass concentration and sized by the OA loadings.



1042

1043 **Fig. 12.** Average composition of PM₁ (pie charts) and OA factors (bar charts) for each cluster. The four
 1044 clusters are: **(a)** northeasterly (NE) back-trajectories (BTs), easterly marine (EM) BTs, southeasterly
 1045 marine (SEM) BTs and westerly continental (WC) during the summer harvest; and **(b)** northerly
 1046 continental (NC) BTs, northeasterly marine (NEM) BTs, easterly marine (EM) BTs and southerly
 1047 continental (SC) during the autumn harvest. The markers on the trajectories indicate 6 h interval.